REPORT DOCUMENTATION PAGE

Form Approved
OMB No. 0704-0188

1. REPORT DATE *(DD-MM-YYYY)*	**2. REPORT TYPE**	**3. DATES COVERED** *(From - To)*
07-09-2007	Dissertation	

4. TITLE AND SUBTITLE

Performance Feedback & Control of Solar Concentrators Using Wave Front Sensing Techniques (Preprint)

5a. CONTRACT NUMBER

5b. GRANT NUMBER

5c. PROGRAM ELEMENT NUMBER

6. AUTHOR(S)
Jason N. Beasley (AFRL/RZSO)

5d. PROJECT NUMBER
4847015N

5e. TASK NUMBER

5f. WORK UNIT NUMBER

7. PERFORMING ORGANIZATION NAME(S) AND ADDRESS(ES)

AFRL/RZSO
8 Draco Drive
Edwards AFB CA 93524-7135

8. PERFORMING ORGANIZATION REPORT NUMBER

AFRL-PR-ED-TP-2007-418

9. SPONSORING / MONITORING AGENCY NAME(S) AND ADDRESS(ES)

Air Force Research Laboratory (AFMC)
AFRL/RZS
5 Pollux Drive
Edwards AFB CA 93524-7048

10. SPONSOR/MONITOR'S ACRONYM(S)

11. SPONSOR/MONITOR'S NUMBER(S)
AFRL-PR-ED-TP-2007-418

12. DISTRIBUTION / AVAILABILITY STATEMENT

Distribution A: Approved for public release; distribution unlimited. (Public Affairs No. 07394A).

13. SUPPLEMENTARY NOTES
Dissertation for submission to Claremont Graduate University/California State University Long Beach.

14. ABSTRACT

The major requirement for using concentrating Solar Thermal devices is the proper placement of the focal spot on the absorber to provide heating of the working fluid to produce thrust or to generate electricity. Without proper placement of the focal spot, either in a spacecraft or ground unit, solar energy is not transferred to the propellant or working fluid or at best case, a significantly smaller proportion of the incident energy is transferred to the fluid.

A control system is needed for ground units to track the Sun across the sky or to track the Sun as the spacecraft maneuvers. The control system would use a fine focus controller after acquiring a general location for the Sun. Optimal focus was defined for a space-based system as 0.1 degree and 0.1 inch in x, y, and z.

The research problem is to: (1) develop a sensor that provides information about the location of the focus beam from the concentrator that also can tolerate the extreme temperatures involved in providing solar heating, and (2) develop the mathematics of a control system that will focus the concentrator in an optimal fashion based on the sensor measurements. The sensor developed in this dissertation solves the temperature issues by using the absorber as a wave front Sensor and imaging that device with a Charge Coupled Device (CCD) to determine the location of the focal beam.

15. SUBJECT TERMS

16. SECURITY CLASSIFICATION OF:			**17. LIMITATION OF ABSTRACT**	**18. NUMBER OF PAGES**	**19a. NAME OF RESPONSIBLE PERSON**
					Dr. Michael Holmes
a. REPORT	**b. ABSTRACT**	**c. THIS PAGE**	SAR	128	**19b. TELEPHONE NUMBER** *(include area code)*
Unclassified	**Unclassified**	**Unclassified**			N/A

Preprint

Performance Feedback & Control of Solar Concentrators using Wave Front Sensing Techniques

By

Joseph N. Beasley

A Dissertation submitted to the Faculty of Claremont Graduate University and California State University, Long Beach in partial fulfillment of the requirements for the degree of Doctor of Philosophy in the Graduate Faculty of Engineering Mathematics.

Claremont and Long Beach
2008

_____
Dr. Hen Guel Yeh, Co-Chair

_____
Dr. Ellis Cumberbatch, Co-Chair

PREPRINT

We the undersigned, certify that we have read this dissertation of Joseph N. Beasley and approve it as adequate in scope and quality for the degree of Doctor of Philosophy.

Dissertation Committee:

PREPRINT

Abstract of the Dissertation

Performance Feedback & Control of Solar Concentrators using Wave Front Sensing Techniques

By

Joseph N. Beasley

Claremont Graduate University: 2007

The major requirement for using concentrating Solar Thermal devices is the proper placement of the focal spot on the absorber to provide heating of the working fluid to produce thrust or to generate electricity. Without proper placement of the focal spot, either in a spacecraft or ground unit, solar energy is not transferred to the propellant or working fluid or at best case, a significantly smaller proportion of the incident energy is transferred to the fluid.

A control system is needed for ground units to track the Sun across the sky or to track the Sun as the spacecraft maneuvers. The control system would use a fine focus controller after acquiring a general location for the Sun. Optimal focus was defined for a space-based system as 0.1 degree and 0.1 inch in x, y, and z.

The research problem is to: (1) develop a sensor that provides information about the location of the focus beam from the concentrator that also can tolerate the extreme temperatures involved in providing solar heating, and (2) develop the mathematics of a control system that will focus the concentrator in an optimal fashion based on the sensor measurements. The sensor developed in this dissertation solves the temperature issues by using the absorber as a wave front Sensor and imaging that device with a Charge Coupled Device (CCD) to determine the location of the focal beam.

A hardware model of the absorber and concentrator was used to generate images for analysis. Images generated with the hardware models are analyzed by first searching the images for intensity areas on the sensor, and then profiles of the intensity areas are integrated to find centroids of the intensity areas. Once the centroid is found for the intensity areas, the controller can generate commands to move the focal beam to proper focus.

Results from this research indicate that the modified wave front Sensor method worked and provides control information to properly control the concentrators to provide optimal heat transfer to the heating fluid.

Dedication

Acknowledgements

TABLE OF CONTENTS

TABLE OF FIGURES

INTRODUCTION

For direct thrust solar thermal propulsion or terrestrial solar heating, proper positioning of the solar focal spot is paramount. Along with positioning information, a sensor system must tolerate the intense heat generated by a solar concentrator. The sensor system developed in this dissertation satisfies both of the previous requirements. The system developed in this dissertation utilizes the thruster – absorber as the focal spot sensor with a Charge Coupled Device (CCD) camera to image the absorber – sensor. Two image processing methods are applied to the CCD images to generate the focal spot location. Once the focal spot is located on an image positioning information and commands are generated to reposition the concentrators. Both methods produce the focal spot information needed to generate positioning information for the concentrator. This dissertation will follow the experiments, research, and analysis utilized for the development of the new solar sensor system. It also introduces the term "blobs" to refer to intensity areas of light reflected onto the tubes of the sensor from the concentrator. These blobs are images of the light in the

concentrator and also are related to the intensity or power being reflected to the sensor.

Chapter 1 Solar Thermal Propulsion Back Ground

The solar concentrator field may be divided into two primary areas of interest: terrestrial-based and space-based. Both types of concentrator can be either imaging or non-imaging and they can be rigid or inflatable.

Some of the applications of solar concentrators include: terrestrial power, space power, material processing, hazardous material destruction, building illumination, space plant illumination, and other applications.

Solar Thermal Power as propulsion has its roots in the work of Krafft Ericke's Solar Powered Spaceship done in 1956. Ericke's spaceship was the first design that utilized a double solar concentrator connected together by a hydrogen powered thruster. Further development of the solar powered spaceship concept was sporadic during the 1950's and 1960's until a single concentrator thruster was developed in 1963. After 1963, the next development of the technology occurred in 1979 with the development of a twin off axis paraboloid concentrator concept, by Rocketdyne.

The solar thermal field was then relatively dormant from 1979 until the Rocketdyne thruster tests of 1984-1991 with a new Rhenium coil cylindrical cavity.

The solar thermal propulsion activity really took off in the 1990's with the development of castable thin films for casting inflatable concentrators. The 1990's also saw the development of rigidized structures for constructing the support structures for inflatable solar concentrators. The year 1997 saw the successful deployment of a 2 X 3 meter inflatable concentrator that signaled that the technology was ready for up scaling. The development activity from 1997 onward has included the manufacture of a mandrel for casting a 4 X 6 meter inflatable concentrator.

Solar Thermal Propulsion (STP) is a promising concept for use in an Orbital Transport Mission, a deep space mission, or other upper stage space missions requiring high Specific Impulse engines. Specific Impulse or I_{sp} is a rocket propulsion term that measures the thrust per unit of propellant expended. Thus STP systems have a much higher I_{sp} than chemical systems of the same size. Since the energy for propulsion is available to the spacecraft in orbit, in the form of sunlight, an STP system would not have to carry both propellant and oxidizer to produce energy for the

upper stage unit. Only an atomic or molecular propellant such as hydrogen would be needed on the upper stage.

The STP system heats up hydrogen in the thruster/absorber and then expands the hydrogen through a nozzle to produce the thrust required by the vehicle. Thus the thrust-to-weight(of propellant) efficiency of the STP system is much better (more than two times better) than the equivalent chemical upper stage as less non-payload mass is needed in the STP system for the same amount of thrust to be developed.[i]

The major difference between a chemical-type thruster or spacecraft and an STP thruster or spacecraft is that the STP spacecraft does not carry the added weight of the oxidizer as the chemical spacecraft. Thus, the STP has a weight advantage over the chemical spacecraft in that a lighter molecular mass propellant is used.

The STP system also has the added task of controlling the solar concentrators. Not only does the spacecraft need to properly point the concentrators towards the Sun while the craft maneuvers in space, it needs to protect them from the exhaust of the spacecraft. These two requirements limit the control region of the concentrators, thus possibly limiting the available power or limiting maneuverability of the spacecraft itself. A final control

requirement is that the focal cone should always be positioned on the aperture closest to the nozzle for effective heat transfer to the propellant.[ii] The focal cone is defined as the envelope of concentrated light that approximates the hyperbola of rotation, whose surface intersects the concentrator perimeter and the boundary of the region of maximum intensity. The focal cone changes shape and position when the concentrator is shifted from the optimal or focused position see Figure 1.

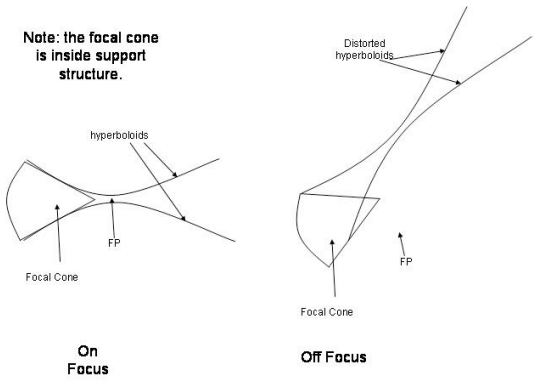

Figure 1 Hyperboloid Construction

The current AFRL concept for the concentrators for a solar thruster is two off axis paraboloid concentrators connected to a central thruster. See Figure 2.

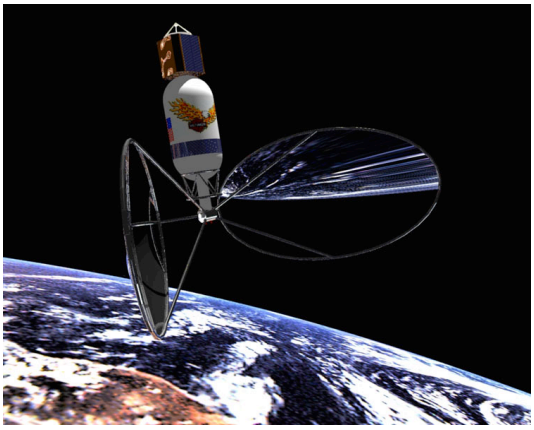

Figure 2 STP SPACECRAFT CONFIGURATION

Each concentrator is connected to the central thruster with a hexapod or Stewart platform offering 6 degree of freedom (DOF) control. The 6 DOF needed are yaw, pitch, roll, x, y, and z. The axes and angles are depicted on the schematic shown in Figure 3.

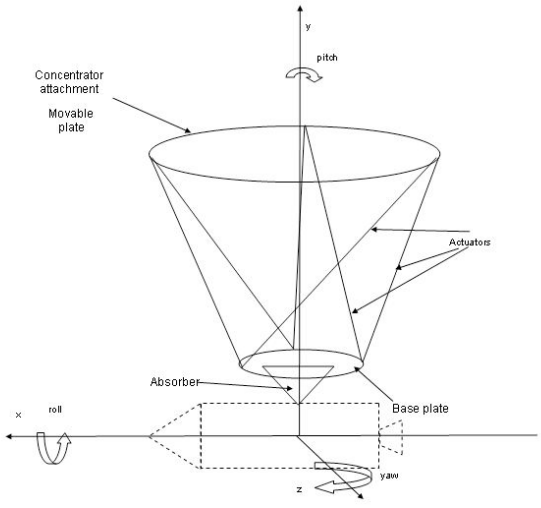

Figure 3 6 DOF Axes For Spacecraft

Optical analysis for a flight demo concentrator system indicated that the required arbitrary angular pointing accuracy is 0.1 deg and the translation accuracy should be 0.1 inch. Coarse alignment is obtained using an on axis detector, such as a Sun tracker or photo diode, which brings the spacecraft and concentrators into a general alignment with the Sun. Coarse alignment, within a few degrees, brings the focal cone into rough alignment with the desired aperture on the thruster.[iii]

A spacecraft's coarse alignment brings the focal cone into rough alignment with the desired aperture on the thruster.[iv] Concentrator control should provide optimum energy transfer to the solar thruster while protecting the concentrator and spacecraft from the dynamic behavior of the whole system.

Concentrator control should provide optimum energy transfer to the solar thruster while protecting the concentrator and spacecraft from the dynamic behavior of the whole system.

Focal Spot:

Proper tracking of the Sun or proper positioning of the focal spot ensures maximum energy transfer to the fluid being heated. To properly track the Sun for maximum heat transfer, the controller requires a sensor with enough

resolution to ensure proper control or better optimal control for maximum heat transfer.

The resulting sensor is shaped like a cone and serves not only as the sensor but also as the solar heat absorber. The method of determining where the focal spot is located using the new sensor system is based on the method used in a Shack-Hartmann optical wave front sensor. The solar sensor developed in this dissertation could be applied to either ground or space-based systems

Chapter 2 Solar Sensor Options[v] [vi]

Most terrestrial Sun trackers were developed to track the Sun from the Earth and rely on open loop mechanical tracking algorithms. That is tracking then was based on mechanical position and vertical position error. Relying on open loop control, these systems were prone to error, because they lacked Sun position error and inertial reference feedback. The open loop control systems are also unable to handle the strut length thermal dependence that feedback systems are able to overcome.

2.1 Thermal based sensors, such as the pyranometer and pyrheliometer rely on thermopiles or thermocouples to measure the temperature rise or difference between the

sensor and its environment. The pyranometer uses an alternating black and white plate connected to the thermopile. The incident solar radiation is reflected and absorbed differently resulting in different temperatures on the black and white areas. The thermopile then can measure the temperature differences between the black and white areas as the measurement of the solar radiation. Another version of the pyranometer uses a Silicon diode as the radiation detector. The diode produces a current directly related to the solar radiation. With the photodiode, the pyranometer is inexpensive, insensitive to temperature or tilt effects and does not require an external power supply.

2.2 Normal Incident Pyrheliometer (NIP): These devices are similar to the pyranometer except that they require a Sun electrically driven equatorial mount to follow the Sun for measuring direct sunlight. The unit consists of a thermopile and a collimator tube that limits incident radiation to a 5 degree circular cone. Incident radiation heats the thermopile which converts the temperature rise into a voltage representing the incident radiation.

2.3 Black body cavities have also been used as absorbers, storage devices and heat exchangers. Black bodies are defined in most physics books as a body that absorbs all radiation that strikes it. Although, no true

black body exists a graphite body is capable of absorbing all but 3 percent of incident radiation striking it. Good approximations of black bodies are cavities having a small aperture or opening through which the radiation enters the cavity. The radiation cannot escape out of the box and increases the box temperature. These devices measure radiation with either a photodiode or thermocouple mounted in the cavity. Once the temperature of the black body is known, the radiation can be determined from Stephan-Boltzmann's law.

2.4 Photo Diodes and Photo Cells are electronic sensors that can be used as replacements for thermocouples or thermopiles in other devices. Photo diodes consist of a Silicon diode in a container that exposes the PN junction to incident light. These devices operate on the internal photoelectric effect. Photo cells are also Silicon-based and are usually operated at short-circuit current. Both photo cells and photo diodes are used to detect visible light.

2.5 Net Radiometers are devices that measure all-wavelength radiation by registering the temperature determined by the balance between absorbed and radiated flux on two horizontal surfaces thermally separated from each other. The top surface of the radiometer has a

coating, usually white, that a thermocouple or thermopile is connected along with a temperature measuring device connected to the bottom surface to measure the two temperatures to determine the difference between reflected radiation and absorbed radiation.

2.6 Calorimeters are devices that measure a temperature increase or difference to indicate radiant energy from the Sun. The simplest type of calorimeter is the "coffee cup" style which is simply two Styrofoam cups inside each other with water and a thermometer in the water to measure the temperature increase. The outside cup serves as an insulator for the inner cup so that the temperature increase in the water can be attributed only to the energy transferred to the water. The medium that is between the two cups is either air or vacuum, with vacuum providing a better insulator similar to a Dewar. Other types of calorimeters exist and use alternatives to the water for the mass that increases in temperature. Some calorimeters consist of a metal chamber with an inner metal chamber for the water or thermal mass. A temperature sensing device such as a thermometer passes through the inner and outer chamber to register the temperature change.

Chapter 3 Solar Sensor Problem Statement

To be useful as a solar sensor both on the Earth and in space the sensor cannot rely on Earth coordinates for tracking information and needs to be robust enough to provide solar tracking while the thruster is maneuvering. The sensor also must be able to handle the high temperatures involved with a solar concentrator that concentrates the sunlight to radiation limited temperatures approaching 4000 degrees Kelvin on the thruster.

The research problem is to: (1) develop a system that provides information about the location of the focus beam from the concentrator that also can tolerate the extreme temperatures involved in providing solar heating, and (2) develop the mathematics of a control system that will focus the concentrator in an optimal fashion based on the sensor measurements. The system presented in this dissertation develops a new sensor that accomplishes both of the requirements for a ground based and a space based solar control system.

NIPs cannot be used for a thruster sensor as they track the Sun mechanically and are tied to Earth coordinates for locating the Sun. NIPs as well as pyranometers cannot function at the temperatures developed by the concentrator. Also, photodiodes and photo cells do not have the temperature capabilities necessary to directly

be used as a focal spot sensor. Photo devices are limited to a temperature of about 85 degrees C while the temperature capability of the pyranometer is about 40 degrees C.

A black body or cavity radiation sensor would not be useful to sense the focal spot as the thruster does not have a cavity on board. Also, the black body or cavity suffers from a lack of response time, being too slow for direct thrust. The black body or cavity sensor is better suited to a thruster that utilizes stored energy for propulsion and does not have a need for continuous thrust.

Calorimeters suffer many of the same problems that the other sensors suffer. Calorimeters need to be in the direct solar radiation path to function so would in fact impair or block the sunlight from reaching the thruster. Also, the materials used in constructing the calorimeter would limit the temperatures that it could withstand to several hundred degrees C instead of the required 3100 degrees K required in a concentrated solar light situation. The need for a thermal mass represented by the water in the coffee cup calorimeter limits the feasibility of using such a device on a spacecraft. Calorimeters can not be used in a continuous temperature update mode that limits them from use as a focal spot sensor. The resolution and

directionality required from the sensor is another limitation of the calorimeter as they cannot provide directional information needed for focal spot tracking.

Radiometers are another type of device that have temperature limitations that would disqualify them from being used as focal spot sensors. The maximum temperature that can be withstood by radiometers is 40-85 degrees C.

The sensor system to be developed solves the temperature issue by using the absorber as a wave front sensor. Since the absorber has to take the high temperatures of the concentrated sunlight, it is already capable of handling the temperature requirements. The CCD images the absorber to determine the location of the focal beam and may use thrust as an additional parameter to improve the focal beam tracking performance.

Chapter 4 Experimental Research

4.1 Fourier Analysis and Focal Spot Simulation

Experiment 1

The appearance of the distribution of intensity in the focal spot is modified by the surface it is scattered from, i.e., the absorber. The detected intensity is complicated by shadows and the specular component of reflection. It is

easy to recognize the absorber but difficult to determine where on the absorber most of the energy is going using just human perception. Furthermore, at different points in the focal spot, the direction of incident light varies. Therefore, as the focal spot drifts across the absorber the distribution of scattered light changes in a complicated way and it is difficult to determine how to correct pointing. This difficulty has been demonstrated in the laboratory in concentrator testing.

Digital signal processing can be used to "de-convolve" the misaligned focal spot image from the scattering distribution of the thruster absorber. In the case of the current section, the sensors used for focal spot placement consist of a coarse alignment sensor for gross movement of the collectors, followed by fine alignment sensors for precise alignment of the focal spot. Proper alignment is determined by examining the shape, size and intensity of the light of the focal spot on the absorber.

Sensors that allow this type of examination and that would handle the high temperatures presented at the absorber are not readily available. Two possibilities are Charge Coupled Device (CCD) arrays and photo diode detector arrays. The CCD array would be positioned out of direct sunlight, using a lens system for imaging, and would

therefore be somewhat protected from the intense heat. The photo diodes as discussed in section 3 would be in direct sunlight and would not be able to handle the high temperatures.

To begin the work, a computer simulation of the focal beam of an off-axis concentrator was used to explore image methods to use on the images for determining the focal spot location.

Computer Simulation:

A C program called Off-axis generates the focal spot information, based upon having a Lambertian target at the focal plane. This program was written by Dr. Michael R. Holmes of the Air Force Research Laboratory, specifically for inflatable concentrators, and provides an "image" of the focal spot target area being illuminated by an off-axis concentrator. Output data generated by offaxis.c represented the focal spot image intensity.

Although, the simulation produces ideal focal beams, using ray-tracing with Monte Carlo slope error simulation, it is an important starting place to prove that the concepts in this paper could work, and supplied important data for analysis to begin.

Since the simulation produced a nearly ideal situation, the focal spot generated resulted in a Gaussian-

type focal spot intensity distribution. Contour and surface plots of the simulation results are shown in Figures 4-7 indicating the Gaussian 3-dimensional nature of the focal beam.

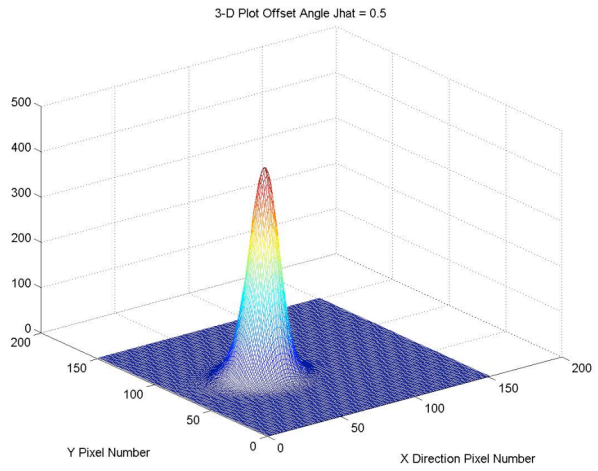

Figure 4 3D PLOT OF FOCAL SPOT JHAT -0.5

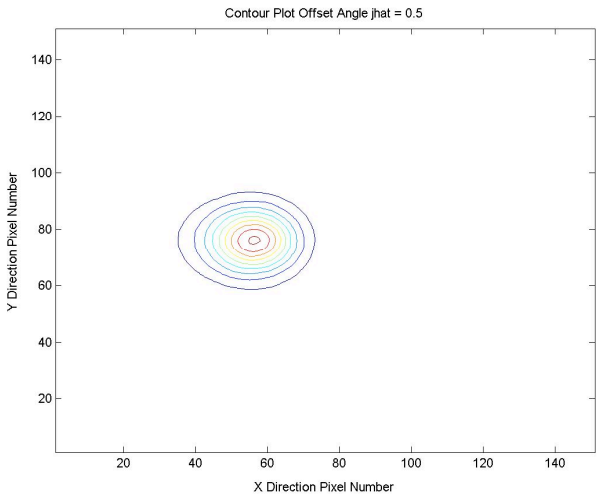

Figure 5 CONTOUR PLOT OF FIGURE 2

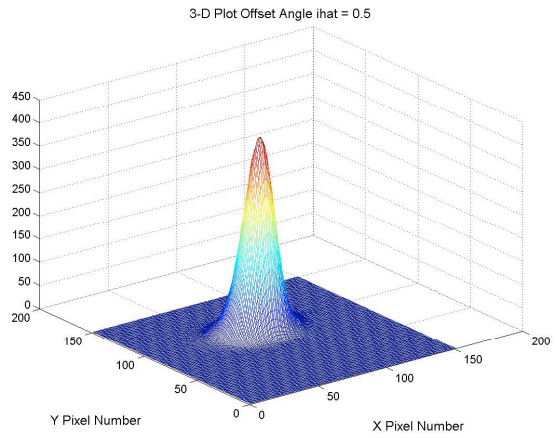

Figure 6 3D PLOT OF FOCAL SPOT IHAT = 0.5

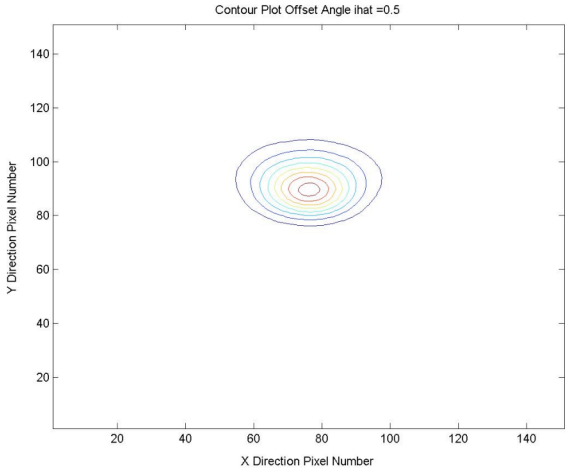

Figure 7 CONTOUR PLOT FOR FIGURE 4

The contour plots show that the focus spot is actually elliptical instead of perfectly circular. The elliptical nature of the focus is due to the off axis nature of the concentrator and will be utilized in the determination of the location of the focus. The parameters for the Sun and concentrator positions are passed to the program through

offaxis.h. By varying the parameters in this file, the various misaligned positions of the Sun and concentrator can be simulated. Of primary concern to this section are the Sun's offset angle parameters. These two parameters change the angular position of the solar disc in the x, (IHAT) and y, (JHAT) directions. See Figure 8 for the geometry.

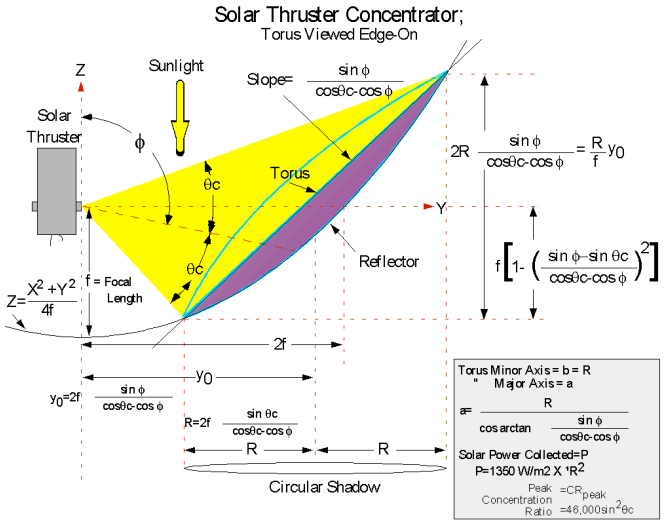

Figure 8 OFF-AXIS PARABOLOID GEOMETRY

The simulation runs for this portion of the dissertation varied these two parameters only. Note that once the data was generated, the image matrix was treated in an X-Y image data plane instead of what is represented in Figure 8 that is the focal spot data image is presented in its own X-Y plane separate from the coordinate system depicted in Figure 8 and depicted in Figure 9. The

specific concentrator modeled in the runs was a 4 X 6 meter Flight Scale Concentrator manufactured by SRS Technologies, Huntsville, AL.

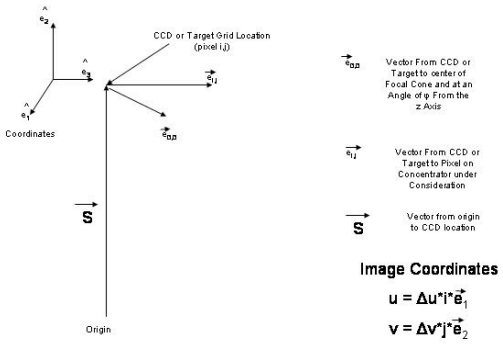

Figure 9 CCD or Imager Coordinates

Analysis Methods:

Once the image data were generated, the data were analyzed using Matlab. Initial analysis used the 2-dimensional Fourier Transform (FT) or Fast Fourier Transform (FFT) as Matlab implements this transform. Equation 1 shows the definition of the 2-dimensional continuous Fourier Transform, with the limits of integration being ±∞. This form of analysis was used as a starting point as it was based upon previous work in one dimensional signal processing and no a priori expectations about what would work. The one dimensional signal processing used Fourier techniques that are expanded to two dimensional or images quite readily.

$$\int_{-\infty}^{\infty}\int_{-\infty}^{\infty} f(x,y)e^{-j(\omega x+vy)}dxdy \qquad (1)$$

The FFT is a fast mathematical algorithm for computing the discrete form of Equation 1; see Equation 2 for discrete FT, utilized by computers to speed up the calculation of FT's in one dimension. In general cases, the 2-dimensional FFT may be calculated by using the 1-dimensional case and applying it to the data twice.

$$X(k) = \sum_{n=0}^{N} f(n)e^{-j\omega_N nk} \qquad (2)$$

with $\omega_N = 2\pi/N$, and summed over n.

However, this effort turned out to be futile as the Fourier Transform of a Gaussian shaped signal is also Gaussian. See Figure 10.

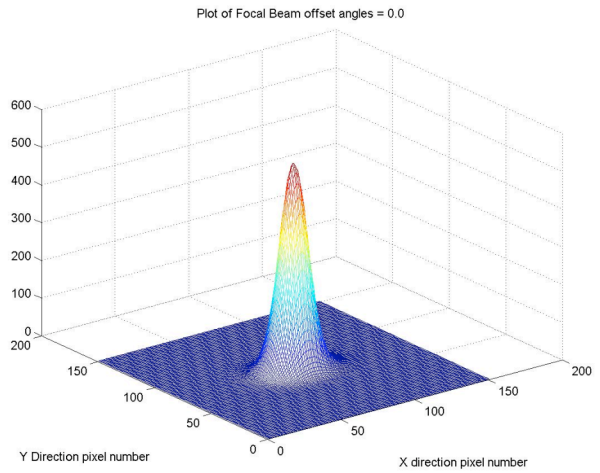

Figure 10 3D PLOT OF FFT FOCAL SPOT BEAM

Although, in the ideal modeling world represented by the focal beam data from the simulation a maximum location could be found, i.e., the beam maximum found using a gradient operation on the original data. A method that could handle a visually more complex image with specular reflections co-mingled with a non-ideal, Gaussian shaped focal spot would need to be developed to be useful in a spacecraft or real case.

The next method of analysis performed was a variant of the Short Time Fourier Transform (STFT) for time signals. The image data was treated as a matrix in Matlab and a vector Fourier Transform (FT) was performed on the matrix. Matlab performs the FFT on a matrix by performing the transform on each column. What this does to the matrix, in effect, is perform a windowed FFT or STFT on the image. See Equation 3, w(t) is the window function in the 1 dimensional continuous transform.

$$F(\omega) = \int_{-\infty}^{\infty} w(t-\tau) f(t) e^{-j\omega_t} dt \qquad (3)$$

In fact, the window happens to be rectangular shaped and is exactly one column size in length. The shift value,τ for each FFT also happened to be one column length, thus making the calculation fairly straightforward to accomplish and actually located at each X value. The result of using the

STFT on the image was a 2- dimensional graph depicting the FT of the image in lines along the Y axis on grid spacing identical to the X axis grid. Thus, the STFT provided a frequency distribution along the Y axis, but local to each X value.

The position of the focal beam was determined by finding the maximum value of the transforms in each direction. These maximums were then used to calculate the amount of correction in each direction needed to re-center the beam. The FFT and STFT approach was chosen to see what could done with the images with no a priori expectations.

Results of Experiment 1:

The results of performing the STFT on various offset angles are shown in Figures 11-16 . Comparing the data plots from the STFT's to the contour plots, Figures 17-19 of the same offset angles, gave the sense that STFT's would provide the needed information about the location of the focal spot in the X and Y directions. Table 1 describes each of the graphs.

Figure 11	STFT X Dir	IHAT = -0.5deg.
Figure 12	STFT Y Dir	IHAT = -0.5deg.
Figure 13	STFT X Dir	JHAT =0.5 deg.
Figure 14	STFT Y Dir	JHAT =0.5 deg.
Figure 15	STFT X Dir	IHAT=JHAT=0.1 deg.

Figure 16	STFT Y Dir	IHAT=JHAT=0.1 deg.
Figure 17	Contour plot	IHAT = 0.5 deg.
Figure 18	Contour plot	JHAT = 0.5 deg.
Figure 19	Contour plot	IHAT=JHAT=0.1 deg.

Table 1

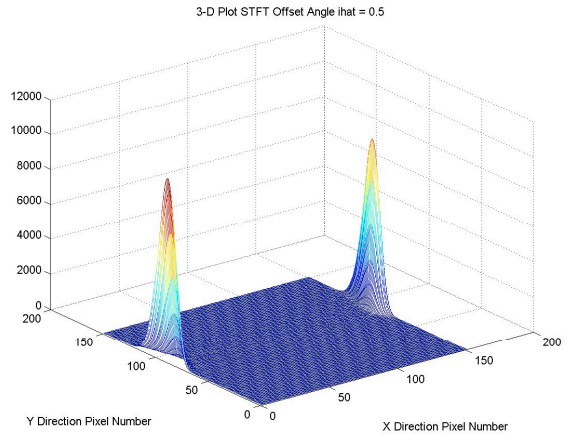

Figure 11 STFT X DIRECTION, IHAT -0.5

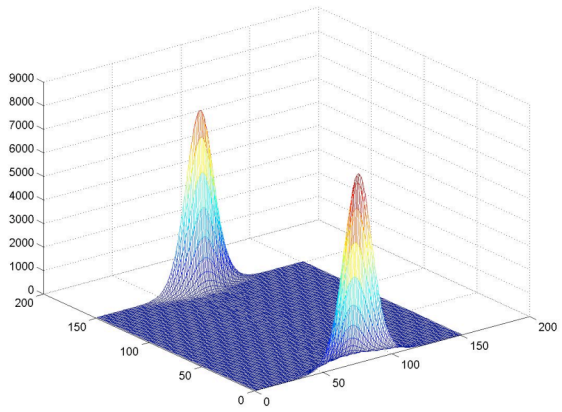

Figure 12 STFT Y DIRECTION, IHAT = -0.5

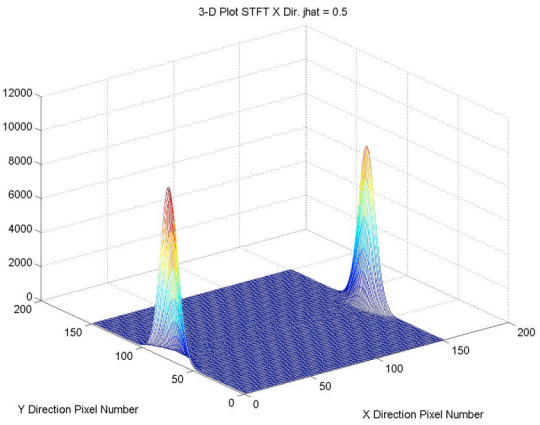

Figure 13 STFT X DIRECTION, JHAT = 0.5

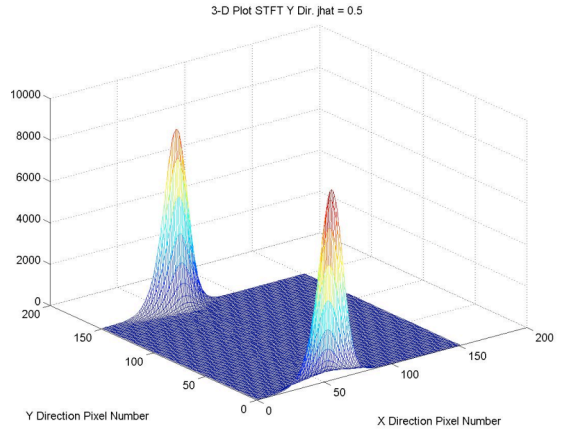

Figure 14 STFT Y DIRECTION, JHAT = 0.5

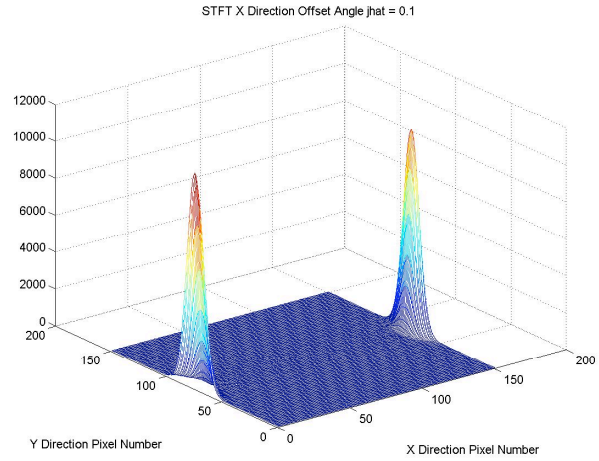

Figure 15 STFT X DIRECTION, JHAT = IHAT = 0.1

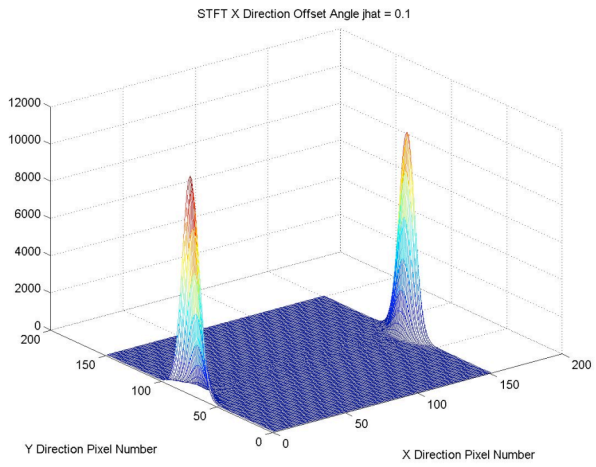

Figure 16 STFT Y DIRECTION, JHAT = IHAT = 0.1

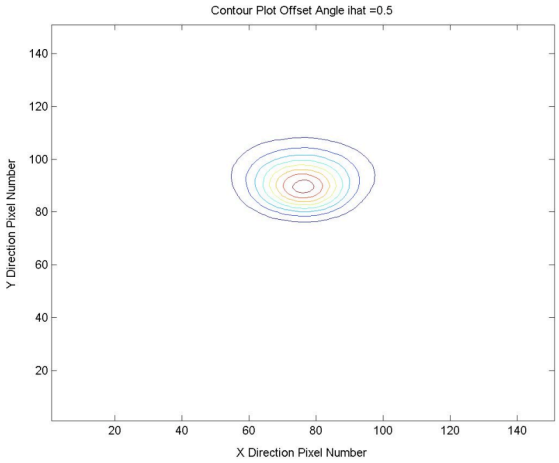

Figure 17 CONTOUR PLOT IHAT = 0.5

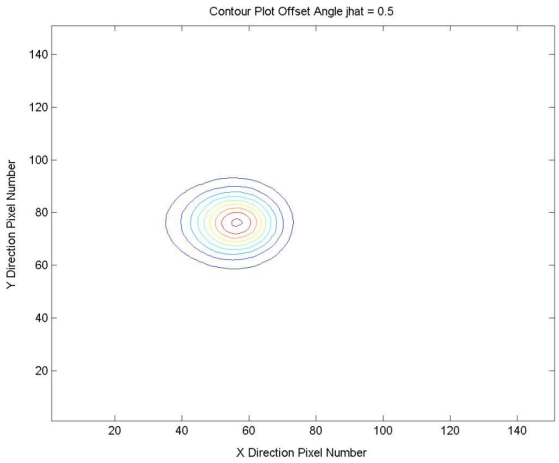

Figure 18 CONTOUR PLOT JHAT = 0.5

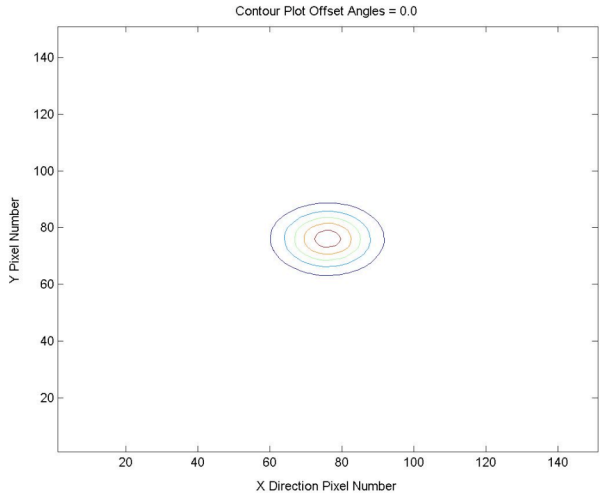

Figure 19 CONTOUR PLOT JHAT = IHAT = 0.1

Computing the STFT first along the Y direction (columns of the matrix) determined position of the beam in the X direction. Computing the STFT along the X direction (using the transposed matrix) determined the location of the focal beam in the Y direction. Finding the maximum of the spectrum and correlating that to the pixel number of

that maximum gave the X, Y location of the focal spot of the focal beam. Table two gives the results of finding maximum values for each of the cases in Figures 11-16 .

Figures 11-12	X pixel Number = 76	Y pixel Number = 90
Figures 13-14	X pixel Number = 56	Y pixel Number = 76
Figures 15-16	X pixel Number = 72	Y pixel Number = 76

Table 2

Each of the pixel numbers in table 2 would be converted to physical measurements using the scaling factors in offaxis.c. The factor in the computer runs presented in this dissertation is 0.226 units of measurement per pixel. The units in most cases are either centimeters or millimeters.

A problem with the use of the STFT in the situations presented, is that some of the offset angles produced only a change in magnitude and the width of the focal beam and not necessarily a change in its X, Y location. The beam was not expected to change peak frequency value, but it was expected to change position in either X or Y. When the beam expanded or narrowed due to the misalignment but did not move the beam in X or Y, the STFT did not provide the

necessary position information. The STFT, however, was able to show that the focal beam width and the maximum value of the focal beam had changed, but only when the offset plot was compared to the zero offset plots, visually.

Summary of Experiment 1:

Data from a computer program was used to generate nearly ideal concentrator performance that was analyzed using the STFT. The results of using the 1 dimensional STFT on images showed promise, thus verifying the concepts, in using the STFT in determining the placement of the focal beam. The STFT's were performed first along the Y axis to determine the pixel number of the maximum beam value in the X direction, then the STFT's were performed along the X axis to determine the pixel number of the maximum beam value in the Y direction. These results provided incentive to continue analyzing the data using the STFT.

One problem that occurred when using the STFT was that in some instances, the beam only changed in magnitude and not direction. In this case, the STFT does not provide sufficient information to get control information.

Using the STFT on simulated data representing the intensity distribution of the focal point was instrumental in showing that the concept of imaging the absorber with

light on it could be used to determine the position of the spot.

Once the location of the focal spot is determined, control inputs should be calculated for output to the hexapod to re-position the spot for better performance. The next section builds on the present section's results by imaging an actual thruster and applying the STFT to the images along with some research into image enhancements that may apply to the images used for control.

4.2 Image Processing of Thrusters:

Since control over the focal spot location on the thruster absorber is paramount in delivering maximum heat to the propellant, it drives the search for a method of locating the focal spot on the thruster and deriving concentrator control inputs to reposition the focal spot to optimize power or heat transfer to the propellant. The sensor and data analysis algorithms used to determine focal spot location are the most important parts in the overall control mechanism. The sensor used in the experiment performed in this section of this chapter was a CCD camera imaging a thruster.

Previous work on this topic[vii] and presented in the previous section, indicated that a short time Fourier transform (STFT) on the image data would lead to the required focal spot location information for data from a computer simulated off-axis concentrator. Also, information in that section indicated that the STFT was not sufficient in cases where the movement of the concentrator did not move the focal spot in X and Y, but only changed the maximum value. The purpose of this effort is to move from the computer simulation to actual thruster data[viii].

Experiment 2:

The setup for the concentrator and data collection system is shown in Figure 20. A 1 m X 2 m elliptical concentrator was utilized for the concentrator as that was the style of concentrator available at SRS Technologies in Huntsville, AL. Figures 85 and 86 in appendix A show photos of the actual concentrator and light source. This type of concentrator was acceptable as the data that was to be collected was only CCD camera shots of the thruster on "Sun" and only a focal spot on the thruster was needed.

The experimental setup in Figure 20 and discussed in this section was optically equivalent to the situation encountered in space utilizing larger concentrators. A

divergent point source located at the other focus of the ellipse was used to simulate the light from the Sun. Because the concentrator was elliptic, the divergent source could be located at the far focus (because light rays emitted from one focus of an ellipse get reflected through the other focus) while the thruster was located at the near focus as shown in the Figure.

The setup in Figure 20 allowed experiments to be performed in a controlled environment that allowed various techniques to be tried before used on a spacecraft. Figure 21 shows a schematic (2 Dimensional) of the setup in Figure 20. Appendix A presents photographs of all of the equipment and setup. A scissor jack platform was used to vary the vertical position of the point source at the far focus. Figure 21 also shows the axes positioning for the source, which is then used in the production of the images presented later. The zero height position of the source is at the focus location of 16.25 inches above the floor of the setup building.

The data collection system consisted of an ST-6 CCD Camera manufactured by SBIG in Santa Barbara, CA and a Sony Vaio computer running SBIG's proprietary image collection software. This software allowed the user to control and

set various parameters of the camera. One parameter under user control was the exposure time for the camera to view the scene. Exposure times were important as they determined whether the signal-noise ratio of the image was sufficient to provide a good image and not saturate the image. The images presented later in this paper indicate the exposure time.

The camera used a 40 mm f.1 lens with a small aperture similar to a pinhole to provide good depth of field. The CCD was spaced from the lens to give the best full view image of the thruster in focus at 1 meter from the thruster. The CCD in the camera measured 23 X 27 micro-meters and had 375 pixels by 241 pixels. As Figure 20 presents, the camera was mounted on the concentrator supporting ring approximately 64 inches away from the thruster surface.

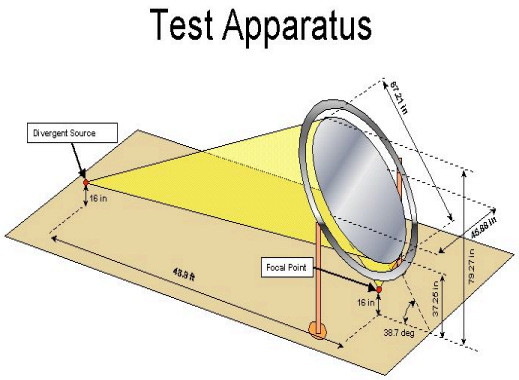

Figure 20 TEST SETUP

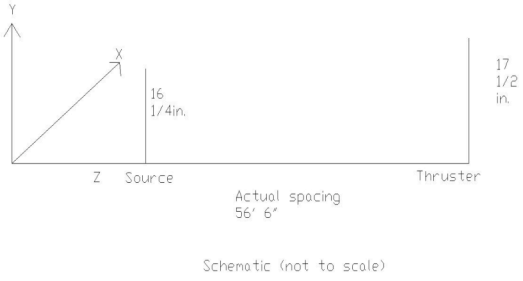

Figure 21 2 D SCHEMATIC OF TEST SETUP

Method of Data Collection:

Since the algorithms must be able to resolve changes in translation of 0.1 inch and 0.1 degrees, the calculation for an angle of 0.1 degree was performed for the setup shown in Figure 20, and was found to be about 1 inch. Therefore, the source light was moved in 1 inch increments in both the vertical and horizontal directions. A standard

measuring tape was used to measure the placement of the source light; measurements were measured to 1 inch lines and could be + or - an eighth of an inch. Once the position of the source was set, the camera was commanded to take an image of the thruster. Each image included taking a "dark" image with the camera element blocked to set a zero image that is subtracted from each light image. Each image was taken for 0.1 seconds. At the time that the experiment was performed, it was thought that the analysis to be performed would provide enough information regarding the specular reflections, that no other exposure times were utilized. Table 3 shows each of the data runs. The maximum vertical limit of the scissors jack was 4 5/8 inches while the maximum horizontal position was 3 inches off of focus. The horizontal limit was a result of how much the scissors jack and point source could be moved on the block before the unit would fall off of the block.

Run Number	Offset Vertical (inches)	Offset Horizontal (inches)	Exposure Time	Comments
1	0	0	0.1 s	Start
2	1	0	0.1 s	
3	2	0	0.1 s	

Run Number	Offset Vertical (inches)	Offset Horizontal (inches)	Exposure Time	Comments
4	3	0	0.1 s	
5	4	0	0.1 s	
6	5	0	0.1 s	
7	0	0	0.1 s	Source off
8	0	1	0.1 s	
9	1	1	0.1 s	
10	2	1	0.1 s	
11	3	1	0.1 s	
12	4	1	0.1 s	
13	0	2	0.1 s	
14	1	2	0.1 s	
15	2	2	0.1 s	
16	3	2	0.1 s	
17	4	2	0.1 s	
18	0	3	0.1 s	Source off
19	0	3	0.1 s	
20	1	3	0.1 s	
21	2	3	0.1 s	
22	3	3	0.1 s	

Run Number	Offset Vertical (inches)	Offset Horizontal (inches)	Exposure Time	Comments
23	4	3	0.1 s	

Table 3: Test information for experiment.

Image Processing:

Mathworks MATLAB software with the Image Processing Toolbox was used to perform the image analysis. Each image was loaded into the MATLAB program along with the one source-off image taken. The source-off image was taken to capture the ambient lighting effects in the SRS high bay.

The methods used to process the images consisted of several steps. The methods used and described next were taken from those methods discussed in computer vision texts. Many computer vision texts develop methods that try to mimic the human eye and mimic human interpretation of those images. Thus histogram equalization was thought to be a necessary enhancement to perform on the images as that would improve a visual interpretation of those images. Also, it was thought that it would be necessary to determine or locate the edges of each of the tubes to

facilitate locating the images of the concentrator on the sensor.

Each image was first enhanced to provide contrast adjustment so that a human could interpret the image and locate various portions of the sensor. Contrast enhancement was thought to be necessary as each image had a very limited range of intensities, as evidenced in a representative histogram shown in Figure 23, so the images' ranges of intensities were stretched to fill the dynamic range. Then each image was filtered using a Gaussian low-pass filter. After low-pass filtering, each image was then filtered using a LaPlacian high-pass filter (LOG—LaPlacian of Gaussian) to provide image edge enhancement. The LoG filtering was thought to help eliminate the histogram problems encountered in the images taken for the experiment.

Although, the LoG filter removes intensity bias, caused by changes in illuminations, it did not help improve the histogram of the images[ix]. This last image, in effect a band-passed image, with the edges enhanced and the noise from the LaPlacian filter reduced by the low-pass filtering was used for further analysis.[x] Finally, the pre-processed and filtered source-off image was subtracted from each

image to remove the effects of the ambient lighting which could add to any bias noted in the image.

The second method used the same pre-processing steps as the first one but substituted an average filter instead of the LOG filter. Each method will be discussed as to its effectiveness in the next section.

Image Analysis:

Figure 22 shows an image with the source located at a 4-inch vertical offset and before histogram equalization. A histogram of the image with a 4-inch vertical offset is shown in Figure 23 and possibly indicates the need to perform contrast enhancement, as most of the pixels lie in the lower portion of the histogram. The need for contrast enhancement was in line with the thought of using elements and theories from computer vision to locate and track the focal spot. As will be shown later in this dissertation, the most important pixel brightness levels are located at the far right of the histogram images, representing the bright white specular reflections of the concentrator. Figures 24 and 25 show the image and histogram after histogram equalization. Figure 26 shows the source-off image after enhancement. Figure 27 shows the final image after LOG filtering and subtraction. It is this final

image that will be used in the image analysis. Figure 28 shows the final enhanced image when the average filter is used for the enhancement process. Each of the images shown in Figures 27 and 28 were then analyzed with the STFT to find out whether the location of the focal spot could be determined. Figure 29 shows the result from using the STFT on the data from LoG filtering of the image.

Results of Experiment 2:

Since LoG filtering is basically a band pass operation on the images, the STFT produces the band pass response of the image and does not provide information for determining focal spot location using the STFT. The STFT results from using the averaging filter were more interesting as far as their use in determining the location of the focal spot.

In both the X direction and the Y direction, pixel numbers for the maximum of the focal spot were determined with ease. The STFT in X and Y directions are shown in Figures 30 and 31 and show that the maximums in each direction on Figure 30 and 31 would, respectively, produce the X pixel number and Y pixel number of the location of the focal spot. The information provided from those two Figures calculations could then be processed to provide concentrator control commands.

A conclusion from this section is that the averaging filter was shown to be better suited when the STFT was used to determine focal spot location. Although the LoG filtering was not as useful, it could still be useful for procedures that do not perform Fourier-type operations, such as spatial-domain operations involving gradients, feature extraction, etc.

Histogram processing is useful when each image is to be interpreted by a human to make sure that the intensities fully populate the histogram thus increasing the ability of the human to discern where the tubes are in the picture to help move the focal spot. Instead of taking images at multiple 1-inch increments, fewer increments and more exposures should be taken to be sure that the histograms are more fully populated. A study of the specular reflection seen at the absorber needs to be accomplished, as the current imaging techniques and analysis do not properly account for the specular reflections. Plus filtering techniques beyond LoG filtering would need to be studied to determine if additional filtering techniques are able to handle the specular reflections and also provide a better means of determining the location of the focal spot.

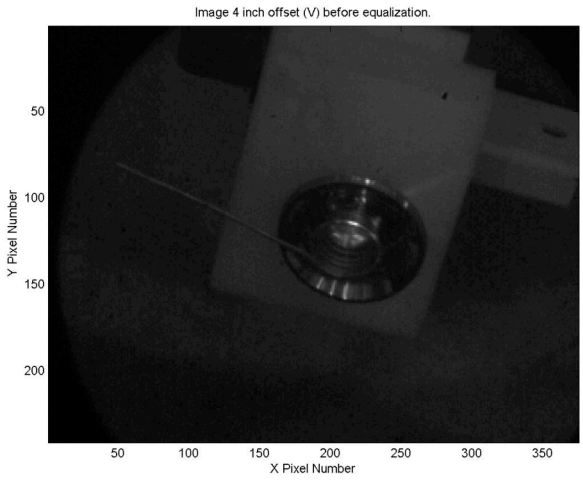

Figure 22 Image Before Equalization

Figure 19A Image in Figure 19 Before Equalization

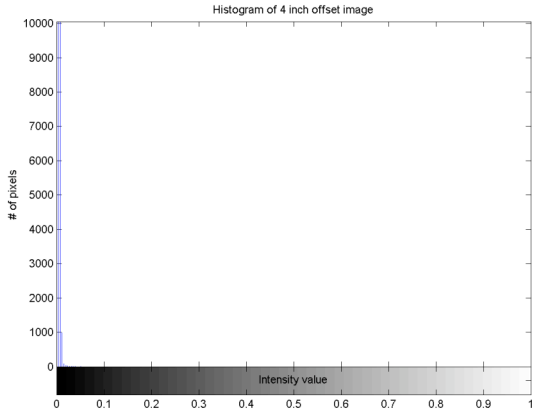

Figure 23 HISTOGRAM 4 INCH VERTICAL OFFSET

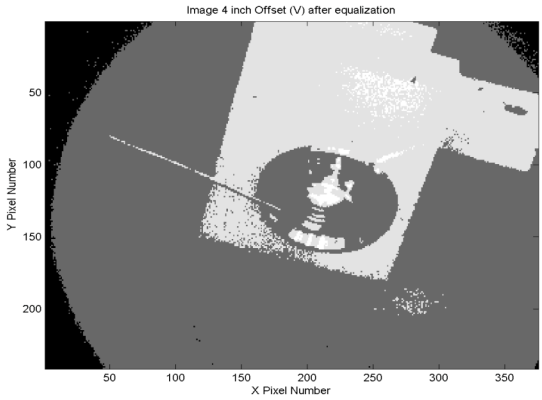

Figure 24 IMAGE AFTER HISTOGRAM EQUALIZATION

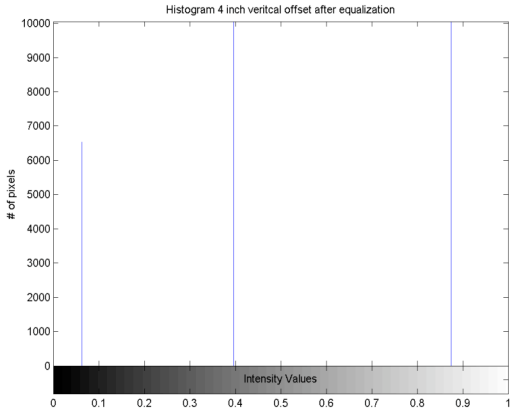

Figure 25 5X3 HISTOGRAM AFTER EQUALIZATION

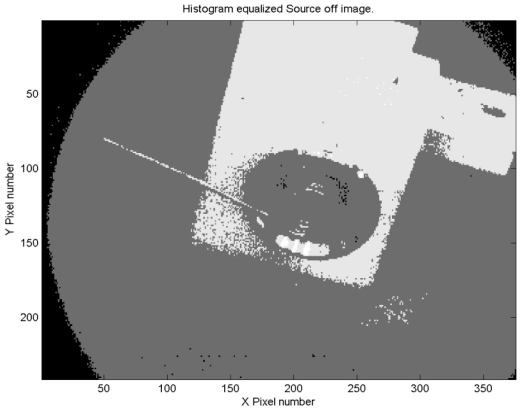

Figure 26 SOURCE-OFF AFTER EQUALIZATION

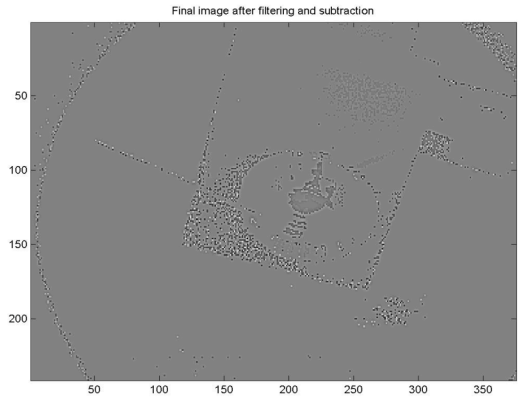

Figure 27 FINAL IMAGE AFTER LOG FILTERING AND SUBTRACTION

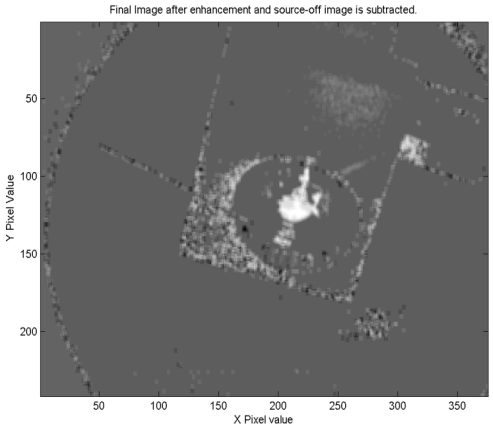

Figure 28 FINAL IMAGE AFTER ENHANCEMENT AND SUBTRACTION

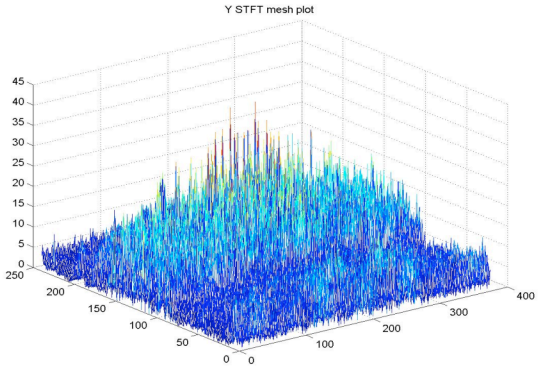

Figure 29 PLOT OF STFT Y DIRECTION LOG FILTERED IMAGE

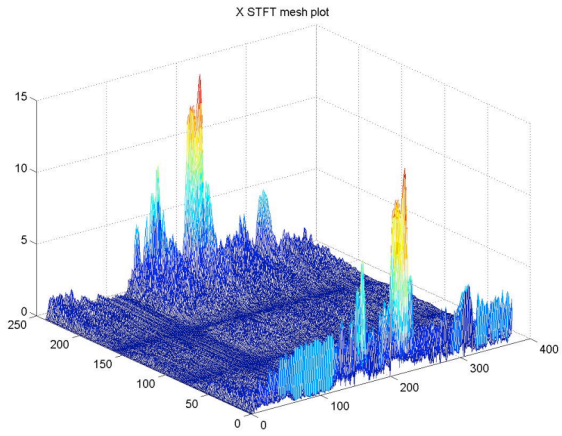

Figure 30 X DIRECTION STFT MAGNITUDE

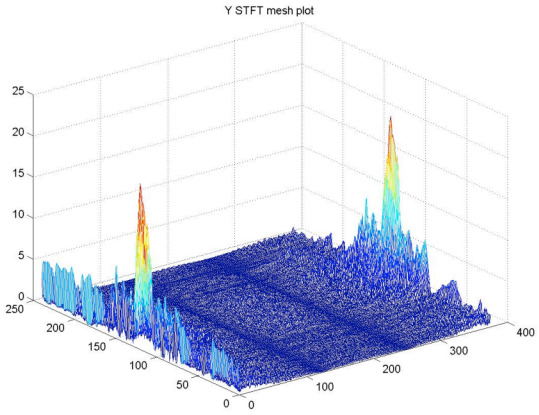

Figure 31 Y STFT MAGNITUDE

The experiment performed and reported in section 4.2, gave promising results in the search for an acceptable device for tracking the focal spot on the thruster. However, another approach was suggested by Dr. Michael Holmes that still used CCD camera but interpreted the image data differently than before, his suggestion also did not require the Fourier transform processing of the images. It also did not necessarily need much enhancement of the

resulting images as discussed in section 4.2. That new approach was to use the absorber as a sensor and process the images similarly to a Shack-Hartmann wave front sensor. Section 4.3 introduces the new sensor and algorithms.

4.3 Wave Front Sensor[xi]

This section describes how the absorber is to be used as a sensor for concentrator control. The sensor is shaped like a cone and serves not only as the sensor but also as the solar heat absorber. The method of determining where the focal spot is located on the sensor uses either one of two methods derived from a Shack-Hartmann optical wave front sensor.

The Hartmann wave front sensor was developed by Hartmann in 1900 and was used for checking optical telescopes for aberrations. It was an array of holes in a plate placed in front of the mirror of the telescope being checked so that light tubes from the array would impinge on the telescope mirror. Two photographic plates were used to collect the light information. One plate was placed just before the focal spot of the telescope and the other one was placed just behind the focal spot. The distance between the plates was chosen so that the light rays would be separated from each other. The path of the light rays was traceable by measuring the centroids of the two images.

Thus, Hartmann was able to determine Figures of merit for various large telescopes.[xii]

Dr. Roland Shack developed the method of replacing the holes of the Hartmann sensor with small lenses or lenslets to improve the capability of the Hartmann sensor when taking images of satellites or stars at the same time as the wave front phase error was being determined. The method was developed while solving a problem with imaging satellites and stars from the Earth. Dr. Aden Mienel's solution was to determine the Optical Transfer Function of the atmosphere at the same time as the image being taken. The Hartmann sensor was not satisfactory as Mienel could not allow the array to cover the aperture of the telescope because it would eliminate the image of the satellite in favor of determining wave front tilt over the imaging of the satellites. Mienel tried to use a beam splitter to take Hartmann images while taking images of the satellites and stars. This method suffered from the weak intensity images of the light rays in the Hartmann sensor.

Shack suggested that replacing the apertures in the Hartmann sensor with lenses would eliminate the problems that Mienel was having with his Hartmann device. The lenslets focused spots onto an image plane such that the displacement of the spots from the ideal position of the

spots indicated wave front tilt.[xiii] Thus, the Shack-Hartmann system overcame the shortcomings of the Hartmann sensor while increasing the sensitivity of the Hartmann device alone. A comparison of the two systems is depicted in Figure 32. The Shack-Hartmann sensor is not suitable for use in tracking the focal spot of concentrated solar rays because of the high temperatures encountered in a concentrated sunlight application.

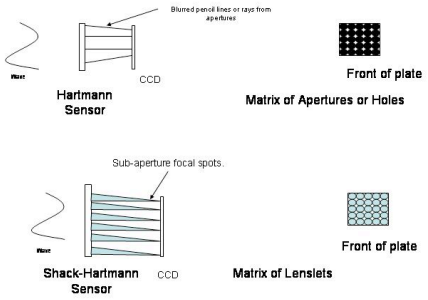

Figure 32 SHACK-HARTMANN VS. HARTMANN

Cylindrical Mirrors

Since the sensor for this application uses coiled tubing as its primary configuration, a brief review of cylindrical mirrors is necessary to understand the reflections generated by the conical tubing absorber. Figure 33 shows the normal situation encountered with the use of a cylindrical mirror. In general a cylindrical mirror will tend to compress an object's reflection along

the length of the mirror. An object's reflection also tends to get larger as the object moves towards the mirror.

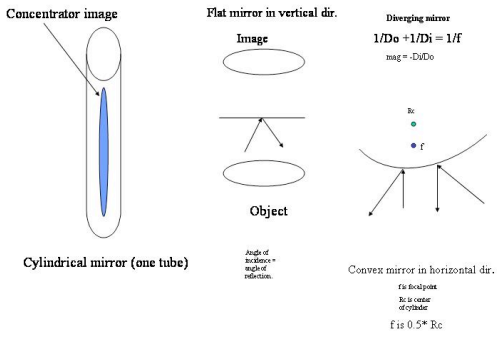

Figure 33 CYLINDRICAL MIRROR

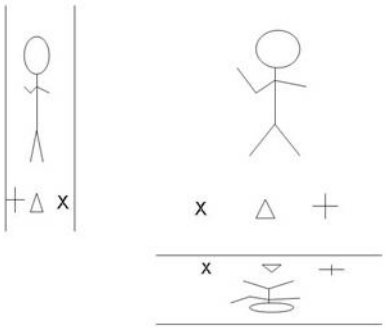

Figure 34 Camera View of Cylindrical Mirror

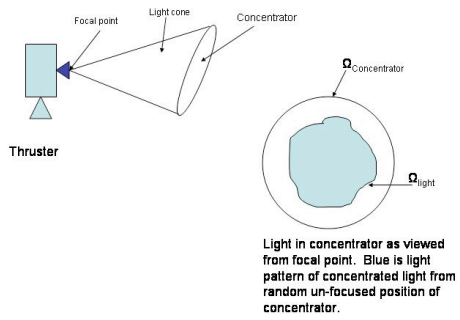

Figure 35 View From Sensor Back to Concentrator

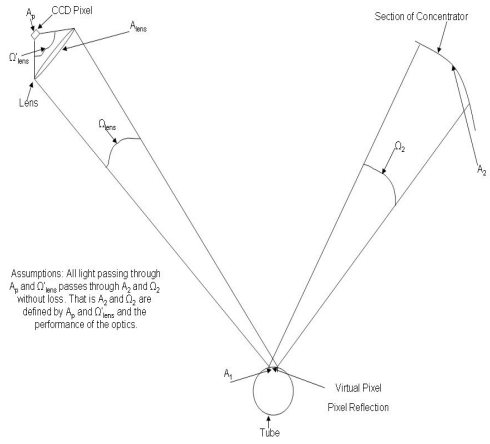

Figure 36 Construction for Flux-tube Calculation

Figure 33 also shows the reflections from the cylindrical mirror along two of its axes. In one axis, in the straight on view, the cylindrical mirror acts like a flat mirror with the light rays adhering to the rules for a flat mirror. That is, incident light is reflected such that the reflected ray returns from the mirror as if it originated at a point behind the mirror, at equal distances to the object; this is also a virtual image. Or the reflection occurs such that the reflected ray's angle is equal to the angle of the incident ray.

On the other axis of the mirror, reflections follow the rules of a convex mirror. That is, the mirror surface has a virtual focus point and all of the reflected light rays appear to come from that focus point behind the mirror surface.

Reflections from other portions of the cylindrical mirror are more complex than the reflections just discussed, however, the overall effect is that the reflection in the cylindrical mirror is compressed along its main axis and appears larger as the viewer moves closer to the mirror. Figure 34 presents the view that a camera or viewer would see when viewing the tubing from a position out of the plane of the Figures and mirror. This viewpoint is important as it is similar to the actual positioning of the sensor, concentrator and camera on the solar thruster.

Figure 35 presents the view of the concentrator from the viewpoint of the absorber looking back at the concentrator. The blue colored regions represent the sunlight that might appear in the concentrator as the focal spot moved into correct focused alignment. That is, the concentrator should be full of sunlight or almost full as the focal spot moves into the proper location on the absorber.

Figure 36 indicates a flux tube calculation to verify that with perfect optics, the CCD camera would be able to view all of the concentrator by imaging the cylindrical mirrors of the absorber. The comparison made in Figure 36 was between the power received by the camera by directly viewing the Sun and by viewing the absorber/concentrator system. Assuming perfect optics it was concluded that the power received via both paths was the same so that we were guaranteed that all of the concentrator would be visible in the camera as well as detectable.

The new sensor system to be described in this chapter combines the effects of the cylindrical mirror and the wave front sensor to allow tracking of the solar focal spot on the absorber.

Sensor Description

The sensor developed in this section consists of a conical shaped absorber made from one quarter inch (¼") metal tubing. For actual application, the tubing would be made from a high temperature metal such as Rhenium or Tungsten. The lens or optic system positions the CCD array to a virtual focal spot location behind the conical absorber. The tubes from the conical absorber act like cylindrical mirrors (toroidal mirrors) in reflecting the sunlight to the CCD. The virtual location is important in

applying the principles from wave front sensing, since the wave front sensor uses either apertures or lenslets projected onto the CCD array.

The lens system then virtually or mathematically positions the array behind the absorber in a manner similar to the Shack-Hartmann system. The major difference between the method being presented in this paper and the Shack-Hartmann system is that the new sensor tries to maximize the number of wave fronts to determine focal spot location, whereas, the Shack-Hartmann system is normally used to optimize one particular wave front.

Algorithm

Each tube would have its own corresponding subset of virtual pixels mapped directly on the CCD array. These subsets would not overlap. Then each image could be processed by utilizing profile information along diagonal lines representing the four quadrants of the circle. (Along the 45 degree angles, say) The areas of maximum intensity could be determined along each profile line. The maximums should occur roughly where the tubes appear in the image as that is where the pixel virtual images are located. The difference or gradient between these areas should give an indication of the direction to the focal

spot. (Almost a centroiding operation on the maximum areas in the image)

By knowing where the center of the absorber is located with respect to the camera (a non-trivial assumption as the camera would probably be mounted to one of the concentrator's movable struts), the computer should be able to generate x, y, z, roll, pitch, and yaw commands for the hexapod controller to move the concentrator to a new position to provide better focus and thus better heating. Figure 37 shows the schematic of the proposed sensor solution.

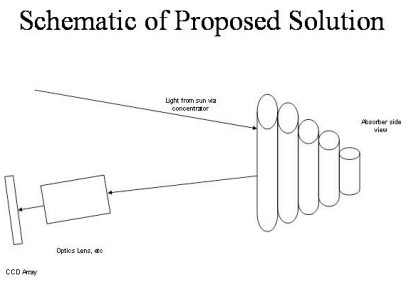

Figure 37 Sensor and Camera Schematic

For the development of the method presented in this section, stainless steel ¼ inch tubes were used for preliminary imaging, while a copper conical absorber with water-cooling will be used for refinement of the method. Figure 38 shows the stainless steel tubes and Figure 39 presents the water-cooled conical shaped absorber as shown

in the schematic in Figure 37. The fluid to be heated is flowed through the absorber tubing and heated by the concentrated light.

Figure 38 STAINLESS STEEL TUBES

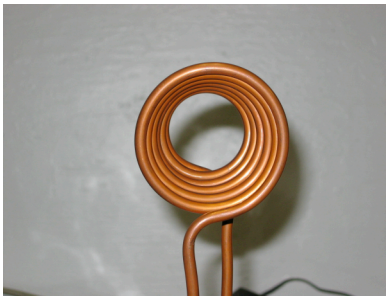

Figure 39 COPPER CONICAL ABSORBER

Calculations

Ray tracing using vectors was used to determine whether the image of the 7-inch diameter concentrator model would reflect off of the tubes and into the aperture of the CCD camera. Figure 40 illustrates the situation and the equation shown could be used in an iteration to find the

angular extremes that would in fact be imaged in the CCD camera. The Figure indicates a theta angle that would be double the angle with respect to the normal vector at the surface of the cylinder. This is happening because of the way things were drawn in Figure 40 and the Law of Reflection: the angle of incidence is equal to the angle of reflection.

A quick calculation using just the rays from the extremes of the concentrator model using the Law of Reflection showed that the CCD matrix or camera was able to view all of the reflection of the concentrator model from the tubes.

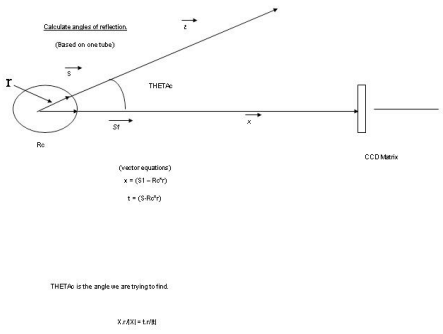

Figure 40 VECTOR CALCULATION FOR REFLECTION ONTO CCD

The field of view of the CCD camera was determined to be 1.4 (495 rows) X 2 (657 columns) inches at a distance of 1 meter from the tubes and can.

Experiment 3

A schematic of the experimental set is shown in Figure 41 and a photo of the experimental equipment is shown in Figure 42.

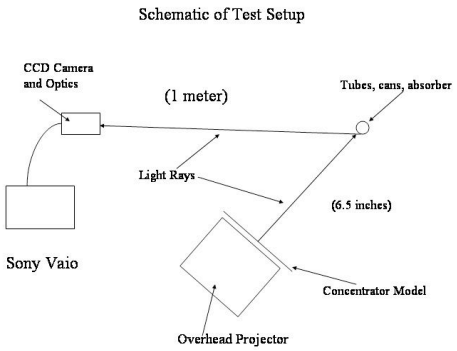

Figure 41 TEST SCHEMATIC

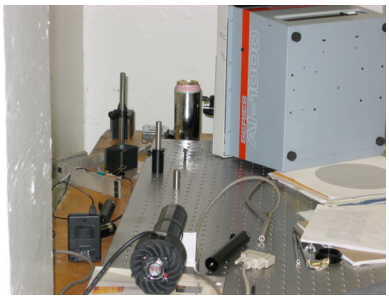

Figure 42 TEST SETUP

The CCD camera used was an ST237 CCD camera manufactured by Santa Barbara Instrument Group. A 657 by 495 CCD matrix with 7.4-micrometer pixels characterizes the ST237 CCD camera. A very small aperture, to gain depth of

field and a 100 mm lens form the optics for the camera. For the experiments discussed in this paper it is focused for objects located one meter away from the lens.

The concentrator model, see Figures 9X4, 10X4, and 11X4, consisted of a 7-inch diagonal circle of white surrounded by a black mask. At the distances shown in Figure 7X4, the concentrator half-angle model was approximately 7 inches in diameter. A standard overhead projector was used to supply light to the concentrator model using a back projection method.

Images of the stainless steel tubes were taken to discern whether an image of the full view concentrator model could be viewed in the tube. Several different exposure times were used as well as different concentrator patterns from full white circles to circles with varying amounts of area blackened to represent various stages of misalignment.

The experiment proceeded by first using one vertical tube, and then two vertical tubes. The three patterns used are shown in Figures 43 through 45. Figure 43 shows the full concentrator pattern, Figure 44 shows pattern one representing a concentrator configuration that would be considered not on focus, and Figure 45 shows pattern number

two with even less white in the concentrator area representing less focus than pattern one.

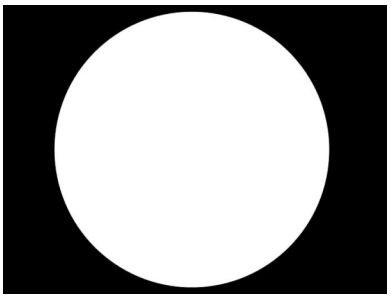

Figure 43 9X4 FULL CONCENTRATOR MODEL

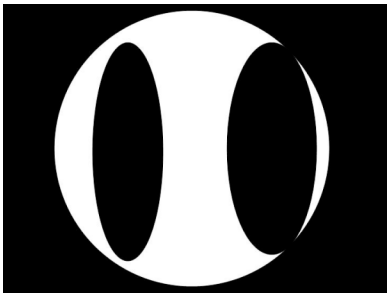

Figure 44 PATTERN ONE MODEL

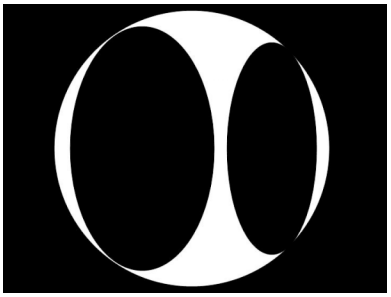

Figure 45 PATTERN TWO MODEL

ONE TUBE

The single tube images indicated that our camera might not have enough resolution to be able to discern between concentrator pattern images. Figure 46 shows the image of

one tube with the full concentrator pattern, and Figure 47 shows the profile through the image.

The images and profiles of the images indicated very little differences between the patterns. The single tube experiment was supposed to show a complete, although distorted image of the concentrator light. At the resolution of the camera, 7.4um pixels focused at 1 meter away from the cylinder did not allow a complete picture of the concentrator model. This experiment may need to be repeated after a camera with higher resolution is acquired.

Figure 46 ONE TUBE FULL CONCENTRATOR

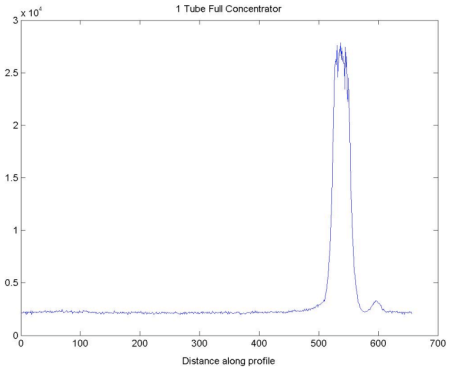

Figure 47 PROFILE FOR FIGURE 46

TWO TUBES

The images from the two-tube experiment are shown in Figures 48-50 and their profiles are shown in Figures 51-53. When each pattern's image and profile are examined, the profiles showed a distinct lowering of the peak intensities seen at each tube location. Pattern number 2 showed the smallest peaks compared to the full concentrator model and to pattern number 1. Since pattern 2 had more black area in the white concentrator area, it was expected to produce less intensity on the tubes. These results indicated that the concept of the new sensor would work as thought. However, since the patterns were not directly related to actual misalignment of the concentrator, no actual position information could be derived from the profile information.

Figure 48 Two Tubes, Full Concentrator

Figure 49 Two Tubes Pattern 1

Figure 50 Two Tubes, Pattern 2

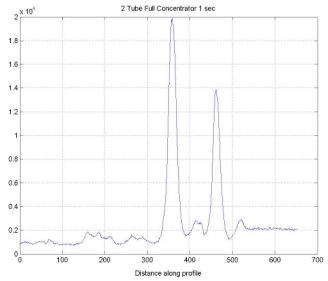

Figure 51 Profile Two Tubes Full Concentrator

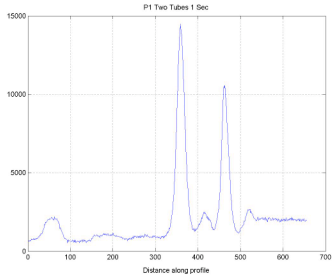

Figure 52 Profile Two Tube Pattern 1

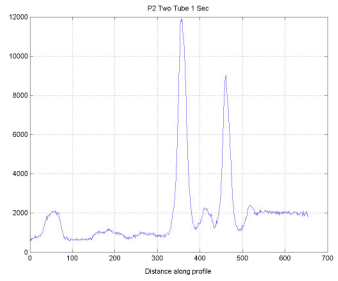

Figure 53 Profile Two Tube Pattern 2

Summary Experiment 3

From the experiments conducted for this section, the concept of using the cylindrical mirrors of the tubing for the absorber as a wave front sensor appears to be feasible and correct. The method of using one tube to look at the concentrator model revealed the fact that the CCD camera being used does not have enough resolution to image the concentrator reflection at 1 meter. The two-tube experiment showed a very promising pattern in that it showed a decrease in intensity in conjunction with a reduction in the white areas Ω_{light} from the full concentrator $\Omega_{concentrator}$ to the other two patterns. Since the patterns did not represent actual misalignment, further work would be needed to make suitable patterns to represent misalignment.

Subsequent work could focus on improving the concentrator models by making them conform to actual

misalignment and to making the black areas able to block more light. A possible error source in the images may be IR light from the overhead projector transmitted through the black paper and causing the intensities to depend more on the IR instead of just the white light. Also, since the projector was not completely black around the areas backlit, scattered light may have entered the CCD and caused intensity changes.

A quick way to make the black outlines darker and opaque to IR would be to either back the model with cardboard or make the patterns out of Aluminum foil. A cardboard mask that masked all but the circular area of the concentrator could be used to improve the extraneous light reaching the CCD camera.

4.4 Concentrator Model

The concentrator model, to model actual misalignment, would have to be constructed such that the dark areas appear at the edges of the concentrator first as the concentrator moves out of focus. At that point the concentrator would have a white center with black edges. Modeling and simulation of the concentrator's ability to capture sunlight was used to determine angles and distances

needed in the imaging of the absorber sensor using an actual concentrator.

The copper coiled absorber sensor would become the primary target for images of the concentrator model. An actual 1 X 2 meter concentrator was available to perform more analysis of the image formed in the concentrator when off focus. Finally, a camera with more resolution was obtained to allow more experimentation with the tubes to investigate the full image of the concentrator providing more insight to the functioning of the cylindrical mirrors and wave front sensor.

A JAVA program, Concentratorv3.java, was written to model the sunlight collected by a paraboloid concentrator. The program listing is in Appendix B. The concentrator model program traced light rays from the target sensor (the absorber) to the Sun. The diagram in Figure 54 shows the vector construction used in the programming of Concentratorv3.java.

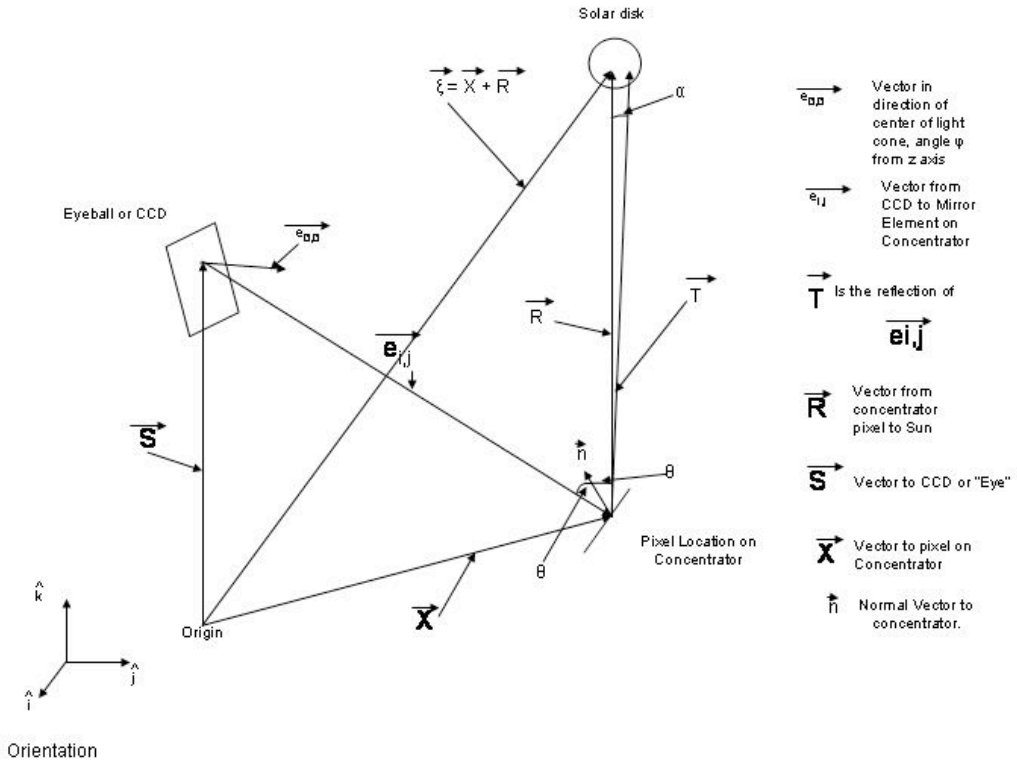

Figure 54 Vector Construction For JAVA Model

The basic operation of the program is that a square grid is built at the eye position which then views the concentrator. The concentrator view is formed on the grid as a projection of the concentrator surface onto the grid plane pointed to by e_{00} and positioned in space using angle from z axis and $_c$, cone half angle using the coordinate system shown in Figure 55. The position of the "eye" or viewpoint vector, initially located at the focus of the paraboloid, is located in space by the vector $\vec{S}$. The

Vector $\vec{X}$, locates each of the incremental mirrors or pixels that make up the surface of the concentrator.

As the program is run, $e_{i,j}$ is incremented through □□ in each direction filling in the grid of the eye or CCD for each vector $e_{i,j}$. A grid point on the CCD is filled if the angle □ between the reflected ray, vector T in Figure 54, and vector R is less than the angle of the Sun, 0.5 degrees. Each run of the program collects information regarding one location on the target or absorber plane.

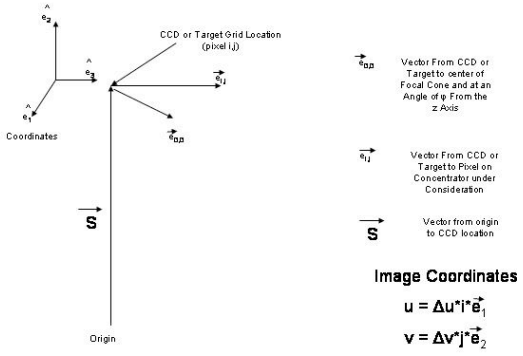

Figure 55 Coordinate System For Target Plane

The datum returned from the program was 1 if the ray could be traced back to the Sun and a 0 if the ray could not be traced back to the Sun. Three Figures are included to show the effects of being off focus by very small

offsets to **S** and to various changes to □and □ $_z$. The Figures are Figures 56, 57, and 58.

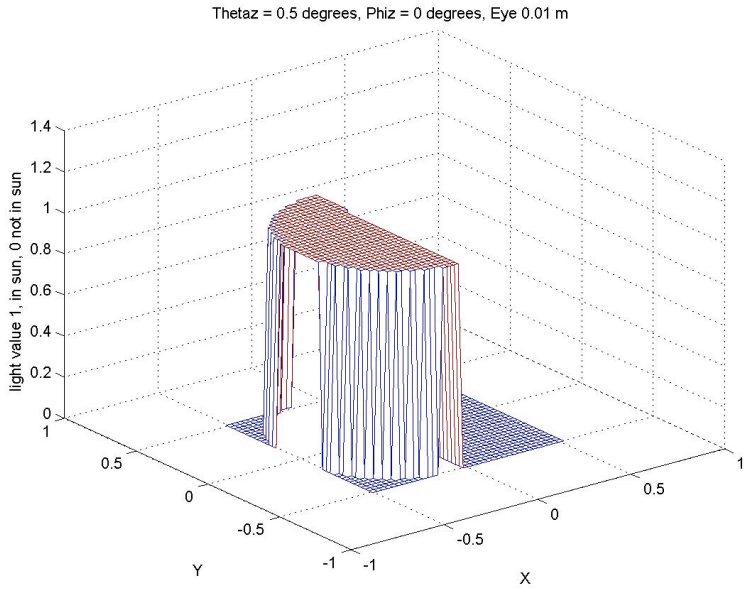

Figure 56 Thetaz = 0.5 Degrees, Phiz = 0, Eye = 0.01m

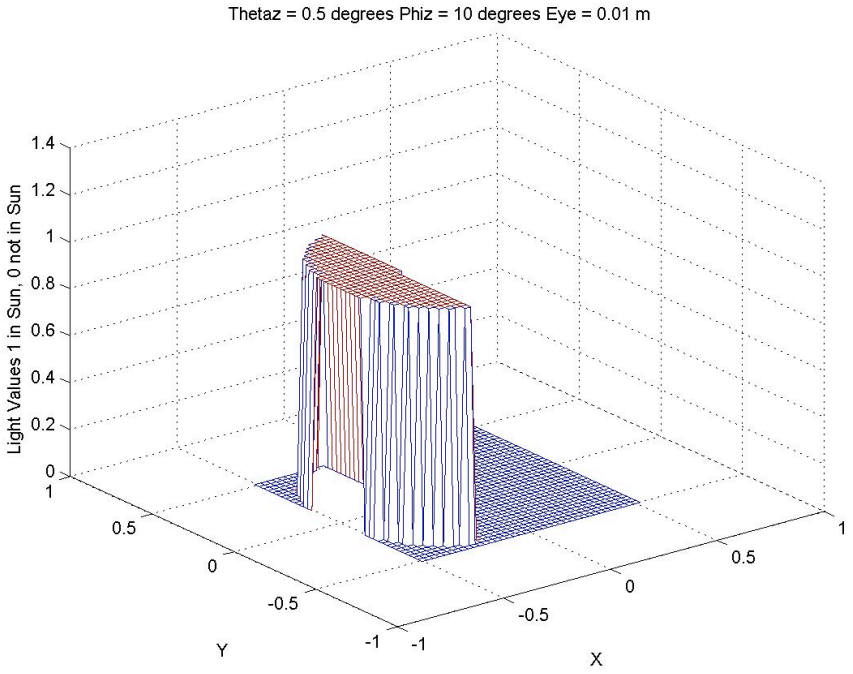

Figure 57 Thetaz = 0.5 Degrees, Phiz = 10 Degrees, Eye = 0.01m

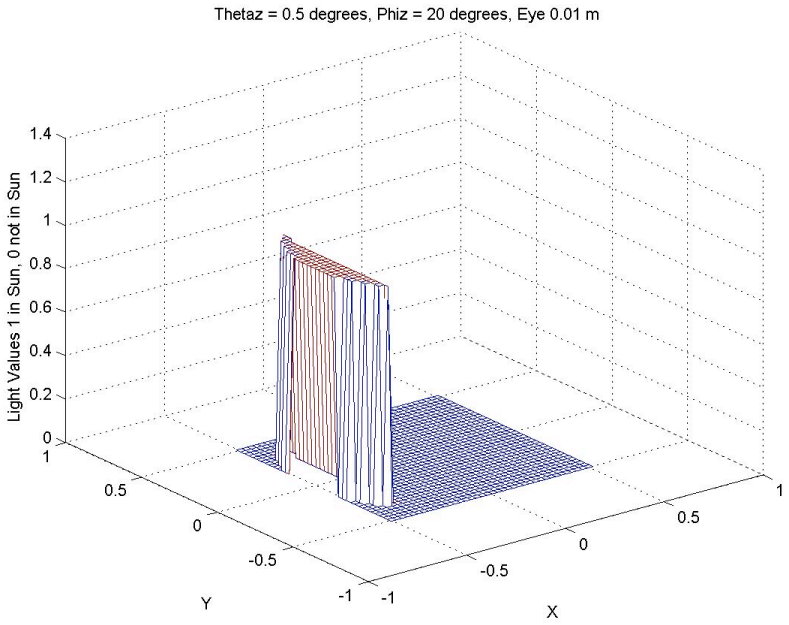

Figure 58 Thetaz = 0.5 Degrees, Phiz = 20 Degrees, Eye = 0.01m

To produce a full picture of the light in the target area, one would have to either run the program multiple times and save the information for collating or modify the program to run multiple view or eye points saving the final data for plotting. The way the program currently functions was sufficient to determine that the control environment for the focal spot location was within one centimeter of the designed focal spot. That is, very little perturbation of the pointing of the focal spot reduced the area of the sunlight being collected and focused on the target or absorber to the point that no light was on the absorber sensor.

4.5 Algorithm Development[xiv]

Control of the position of the solar concentrators to ensure proper heating of the thruster is paramount in STP. Prior work settled on an arbitrary control requirement of 0.1 degree in angular position and 0.1 inch in translation[xv].

Continuing from the definition of I_{sp} from the section on solar thermal propulsion background, I_{sp} is the thrust divided by the propellant expelled in the exhaust.

$$I_{sp} = \frac{\left|\vec{F}\right|}{\dot{m}} = \frac{1}{\dot{m}}\left|\frac{d\vec{p}}{dt}\right| = \frac{1}{\dot{m}}\dot{m}v_e = v_e \tag{4}$$

In 4, v_e is the exhaust velocity. From 4, the expression for the power developed by the exhaust stream of the thruster is shown in 5.

$$P = \vec{F} \bullet \vec{v} = \frac{1}{2}\dot{m}I_{sp}^{\ 2} \tag{5}$$

Equation 5 can be related to concentrator power input P_{in} to the thruster and the thruster loss mechanism η_t as follows in equation 6.

$$P_e = \eta_t P_{in} \tag{6}$$

For the concentrator portion of P_{in}, the equation for the power is in equation 7 with $I_0 = 1350\frac{W}{m^2} \pm 50\frac{W}{m^2}$ at Earth with aperture area A_c.

$$P = I_0 A_c \tag{7}$$

The power transferred to the thruster is related to the intensity of the light collected by the concentrators. The power in equation 7 is modified as the thruster reflects some power away from the thruster and radiates energy at the thruster's black body radiation temperature. The power into the thruster is then shown in equation 8.

$$P_{in} = \varepsilon A\left(I_{in} - \sigma T^4\right) \tag{8}$$

Where ε is the emissivity of absorber area A, σ is the Maxwell- Boltzmann constant, I_{in} is the input power density from concentrator to absorber A, and T is the temperature of the absorber and propellant. Equation 8 is a simple one dimensional expression for the power into the thruster.

The assumptions for equation 8 are that the thruster has a uniform temperature over A, the temperature over A is the same for the propellant, and ε is equal to 1 minus the reflectivity. Otherwise equation 8 becomes an integral over the flow path. In equation 8, I_{in} is found by relating

the solar power density with effects of the optical path through the concentrator as shown in 9.

$$I_{in} = \tau_c C_r I_0 \tag{9}$$

Where τ_c is the transmissivity of the concentrator, $C_r = \frac{A_c}{A}$ and A_c is the area of the concentrator aperture and A is the area of the thruster/absorber, and I_0 is the solar power density at Earth orbit. From equations 9 and 6, the power at the exhaust stream is shown in equation 10.

$$P_e = \eta_t \varepsilon A\left(\tau_c C_r I_0 - \sigma T^4\right) \tag{10}$$

Equations 4 and 10 may be used to find thrust F as a function of I_{sp}, T, and I_0.

Relating the power to the exhaust power, P_e to the misalignment angle of the concentrator is a problem solved numerically using the concentrator code written by Dr. Holmes called offaxis. Figure 59 shows the result for several angles of misalignment. Using values from Figure 59, Figure 60 plots the intensity versus misalignment angle. Figure 60 shows that the power density decreases considerably at 0.2 degrees of misalignment.

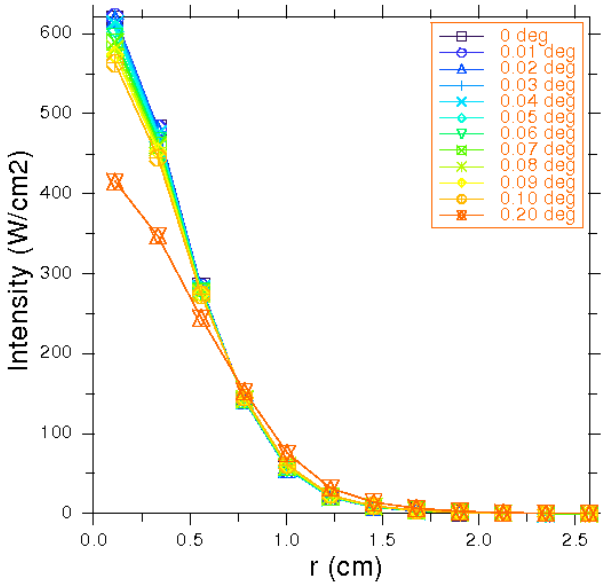

Figure 59 Peak Power Density vs. Radius Off Focus

The peak power at 0.2 degrees of misalignment is approximately 2 dB down and indicates a likely cutoff point for this discussion. Therefore, most of the work presented in this article pursued a 0.1 degree of misalignment target value for maximum power transfer to the thruster.

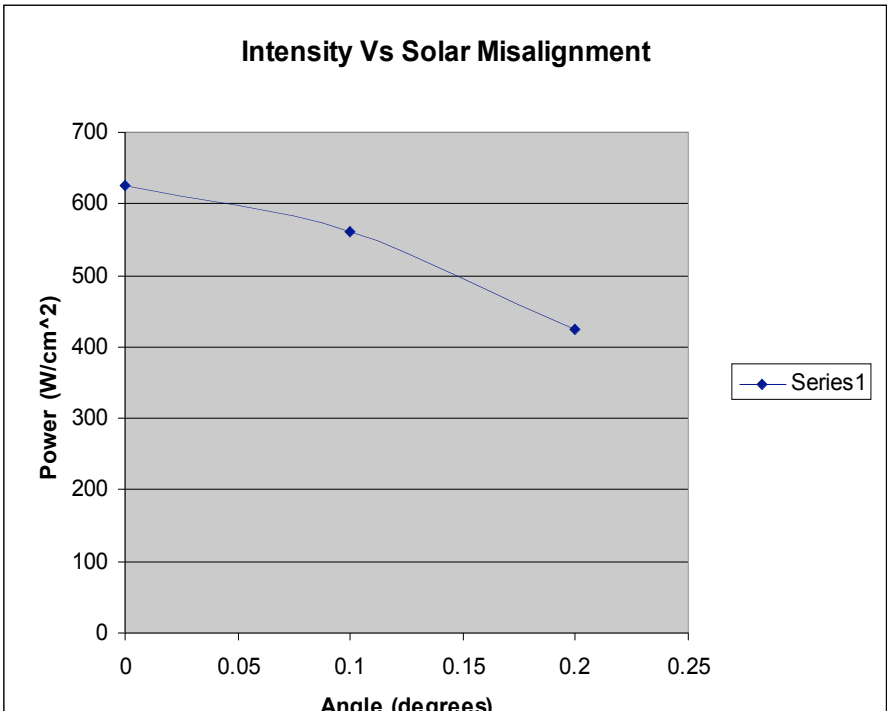

Figure 60 Intensity vs. Solar Misalignment

Section 4.3 presented the idea of using the absorber of the thruster as a sensor for tracking of the focal spot on the absorber. This section presents two algorithms used in determining the location of the focal spot using the absorber as the primary sensor. Both algorithms utilize concepts developed from studies of the Shack-Hartmann wave front sensor. The first algorithm described uses correlation and masking for locating and tracking the focal spot. The second algorithm simplifies the method in algorithm one to using area moments for tracking sunlight.

System Description:

Since section 4.2 presents the hardware being used for focal spot tracking in detail, a brief summary of the components will now be presented for use in this section. The schematic of the hardware is shown in Figure 71 and consists of a CCD camera and a conical shaped tubular absorber.

The new sensor and algorithms are based on the Shack-Hartmann wave front sensor with the holes and lenslets replaced by the cylindrical mirrors of the current system. Sunlight reflecting on the absorber tubing is imaged by the camera for analysis instead of imaging the array of holes or lenslets of the Shack-Hartmann device.

The thruster tubes serve as high temperature mirrors or "lenslets." The absorber takes the heat from the sunlight and conducts it to the Hydrogen gas for use in providing thrust. Differences in location of light and how much light is reflected from the tubes are used to determine the focal spot location error for use in a feedback control system.

Two or possibly three different algorithms will be used to locate the focal spot error from the images of the tubes. Different algorithms were deemed necessary because of the 0.1 degree arbitrary control requirement and not having one universal algorithm that covered the three regimes of focus (sunlight more than 5 diameters off focus), intermediate focus (approximately 5-3 diameters off focus), and fine focus (2-1 diameters off focus).

Algorithms:

METHOD ONE:

The image processing portion of the focus control system was developed along two paths. The first method to be discussed is the more general method using correlation, while the second method is less general based on area moments and area centroids similar to one version of the Shack-Hartmann analysis. The flow chart in Figure 61 shows the sequence to be implemented for solar concentrator focus control.

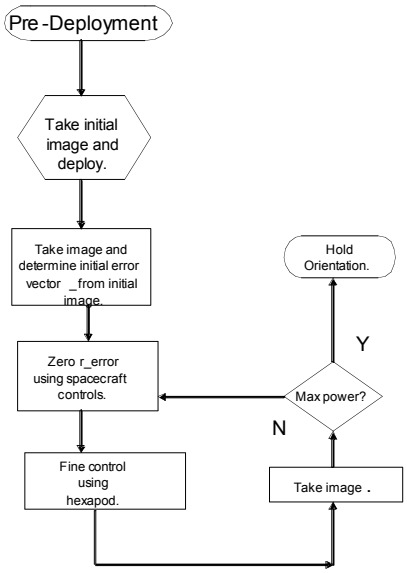

Figure 61 Flow Chart of Sequence

Figure 62 illustrates the diagram of the system after deployment and before coarse focus. The method for coarse focus, which is not discussed in this dissertation, works on minimizing $\vec{\xi}$ to get to the situation shown in Figure 63. The situation is then the initial position for the fine focal controller, the focal spot is located in the general area of the sensor but not on the optimized spot and the system is not thrusting. Thus, after deployment, the camera is pointed at the absorber and the concentrator is positioned facing the Sun. This situation is then defined as the initial position for the coarse control algorithm shown in Figure 62.

With the addition of a stored image of the absorber in the on-Sun and on-focus designed and geometric configuration, the control algorithms begin.

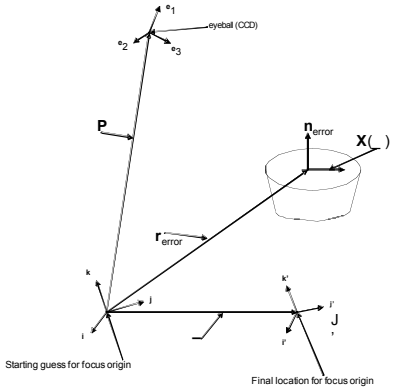

Figure 62 Starting Coordinates For Coarse Focus

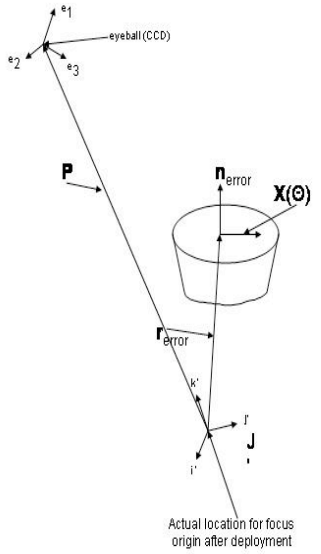

Figure 63 Fine Focus Start Coordinates

At the start of the control program, after coarse focus, the control computer has the initial geometric designed configuration and initial image stored in memory.

These initial conditions also define an initial coordinate system as displayed in Figure 63. Also stored in the control computer are masks to be used in computing where the focal spot is currently located each iteration.

The correlation or the lack of correlation at the masked areas indicates the current location of the spot and indicates the direction of travel required to reduce the mismatch. The overall process for this control algorithm follows image correlation or scene matching from computer pattern recognition[xvi],[xvii],[xviii]. Both procedures follow a similar mathematical development to that of correlation between masked areas of the test image with the image of the on-focus image. Optimization would be utilized to find the optimal and correct focal spot location.

From Figure 63, $\vec{r}_{error}$, $\vec{p}$, $\vec{X}(\theta)$, and $\vec{n}_{error}$ are the primary vectors in the development of the algorithms. When the system is deployed on orbit, the initial position of the concentrator, camera, and thruster determine the initial origin and coordinate system. $\vec{r}_{error}$ is the vector that determines the location of the image in the original coordinate system for the focus spot. $\vec{n}_{error}$ is the vector normal to the plane at the current image location at $\vec{r}_{error}$. $\vec{p}$, is the location of the camera or "eye-position" with

respect to the original coordinate system. Finally, the vector $\vec{X}(\theta)$ represents areas of the images that are regions of interest for locating the focal spot. The regions of interest in the case of these algorithms would be the thruster itself or the individual rings of the absorber. The required accuracy of focal spot location determines whether the thruster as a whole would be the region of interest or the individual rings.

For the imaging portion of the process, the vector $\vec{X}(\theta)$ in the proceeding paragraph would have to be projected onto the CCD camera image plane. The method used for this operation is based on pinhole optics and perspective projection. The CCD camera utilizes a pinhole-like or small aperture for its almost infinite depth of field. A lens is positioned just behind the aperture to focus the aperture image onto the CCD matrix in the camera. With these optical parameters the projection of $\vec{X}(\theta)$ onto the CCD matrix with coordinates (a,b) is determined using the following equations.

$$a(\theta) = \alpha * \left(\left(\overrightarrow{X(\theta)} + \vec{r}_{error} - \vec{p}\right) \bullet \hat{e}_1\right)\left(\left(\overrightarrow{X(\theta)} + \overrightarrow{r_{error}} - \vec{p}\right) \bullet \hat{e}_3\right) \qquad (11)$$

$$b(\theta) = \beta * \left(\left(\vec{X}(\theta) + \vec{r}_{error} - \vec{p}\right) \bullet \hat{e}_2\right)\left(\left(\vec{X}(\theta) + \vec{r}_{error} - \vec{p}\right) \bullet \hat{e}_3\right) \qquad (12)$$

α and β in equations 11 and 12 are scaling factors determined by the CCD pixel size. The $\hat{e}$ vectors are unit vectors located at $\vec{p}$ defining a coordinate system at $\vec{p}$ for the camera.

Now that the image and system coordinates and vectors have been defined, the correlation function is derived. The image taken by the CCD will be denoted I(a, b) and is a function of (α, β) as expected. W (α, β) will represent the image or sub-image that we are trying to match. For example, W (α, β) would represent the ideal on-focus image or it could represent only a portion of the ideal image such as specific rings of the sensor. The L_2 norm will then be utilized to calculate the minimum distance between W (α, β) and the current image.

$$E(m,n) = \left(\sum_{j=1}^{J} \sum_{i=1}^{I} \left[I(i+m-1, j+n-1) - W(I,j) \right]^2 \right)^{0.5} \qquad (13)$$

Where E(m,n) is the measure of distance at coordinates (m,n)

Equation 13 also assumes that W is smaller than the image I, but that does not preclude using a W that is equal to I in size. Squaring and expanding both sides of equation 13 while using the assumption that the energies in W and I are constant and very small, the correlation of W and E results as shown in equation 14.

$$E^2(m,n) = -2 * \sum_{j=1}^{J} \sum_{i=1}^{I} I(i+m-1, j+n-1) * W(i,J) \quad (14)$$

Multiplying equation 14 by -1/2 generates the correlation R(m,n) at (m,n) as shown in equation 15.

$$R(m,n) = \sum_{j=1}^{J} \sum_{i=1}^{I} I(i+m-1, j+n-1) * W(I,j) \quad (15)$$

Finding the maximum value for R(m,n) will determine the best location in the image that matches W. Finding the X,Y location of the maximum value for R(m,n) and determining the difference from that location to the location of the autocorrelation of the on-focus image determines which direction to move the image to match the maximum correlation. Once the difference between the autocorrelation of the on-focus image location and the point of maximum correlation is found, the control system would move the concentrators to reduce this difference. Equation 15, correlation was thought to be sufficient for determining the location of the focus.

MASKS:

Several different masks were generated, using a free hand drawing method, to help determine which masks were best. Best in this usage means that the masks were best suited to determining the offset distance from the focus location. Several masks that were used with the tubular absorber are shown in Figures 64, 65, and 66. Similar masks

were used with the loop of tubing that replaced the absorber for testing.

The difference in the masks was which ring of the absorber was used in preparing the mask. For the outer ring mask, the outermost ring of the absorber was used as the masking area and thus enclosed a bigger area of the image than that covered by the inner ring mask. So although the masks in Figures 64 and 65 look alike, they, in fact, cover very different regions of the images.

The mask in Figure 66 was thought to be able to isolate a portion of the outer ring for consideration. In actual practice, it matched too many intensity levels to be of use, especially once the light got less than 4 diameters off of focus. In other words, Figure 66 could not be used to discriminate below about 4 diameters as its correlation was smeared and did not produce impulse-like behavior at correlation.

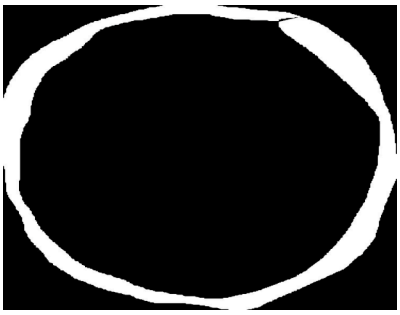

Figure 64 Outer Ring Mask

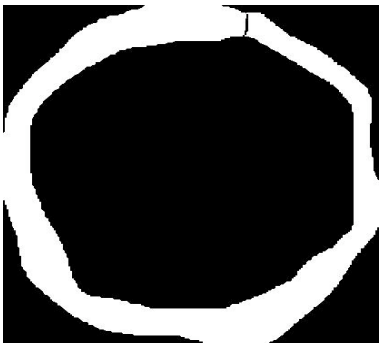

Figure 65 Inner Ring Mask

Figure 66 "Banana" Shaped Mask

METHOD TWO:

The second method for determining focal spot location is by measuring light area moments in the image. This method is derived based on a modification of the Shack-Hartmann wave front sensor using cylindrical mirrors instead of lenslets to register light areas[xix]. Images of the concentrator can be seen in each coil of the absorber. Whether a particular image on the tube, denoted as a "tube blob" is bright or dim depends on how close the tube is to the focal point. Image area moments are then used to

quantify focus for individual "tube blobs." The derivation also follows from a discussion of area moments and centroids from mechanics[xx],[xxi]. An image is acquired via the CCD camera and a threshold is applied to the image for further processing.

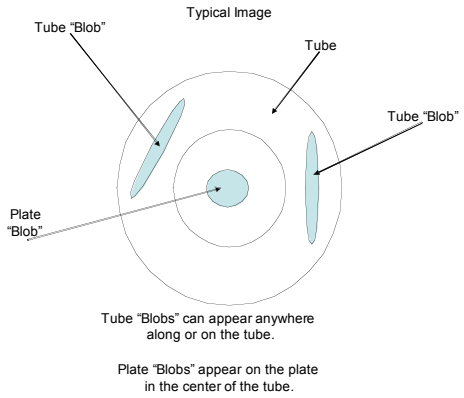

Figure 67 Generic Light Patterns in Image of Sensor

Figure 67 shows a generic schematic of light blobs from an image of the sensor. As explained earlier, each tube "blob" is an actual image of the light from the concentrator. The shape and intensity area of each tube blob is related to the amount of light in the concentrator being concentrated to that area of the tube. Calculating the area centroid of the images in the tubes determines where the focal spot is located on this iteration of the algorithm and knowing where the centroid of the focal spot is located for this iteration determines which direction

the control algorithm needs to move the concentrator to move the centroid to the center of the sensor.

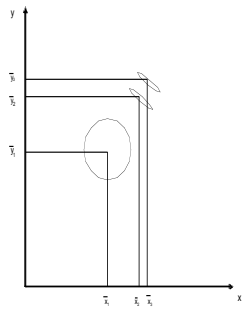

Figure 68 Light in Image From CCD

Figure 68 shows the situation that might occur once the CCD acquires an image. A coordinate system for the image is setup as shown in Figure 68. The image is then processed by first thresholding the image and then calculating the area moments for each light area. The threshold is set, at least in the ground experiments, by visually making sure that the lighted areas in the sensor tubes do not overlap into the area of the secondary concentrator and contain approximately 95% of available light in the images reflected from the concentrator when on focus. On flight another method of preventing overlap would be needed, possibly a measured area of the absorber beyond which the controller would ignore. Once the image has been thresholded, the area moments are calculated and

an average or overall centroid is calculated as the location of the focal spot on the sensor.

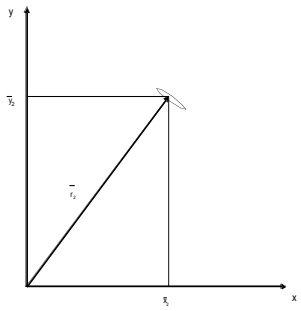

Figure 69 Calculation Schematic

Figure 69 is an ideal schematic of the calculation for one of the ellipse shaped light areas. The light area is located at $\vec{r}_2$ and the area calculated as (±a*b)/4, where (a) is the major axis of the ellipse and (b) is the minor axis of the ellipse. Position vector $\vec{r}_2$ is the vector from the origin to the center of the ellipse.

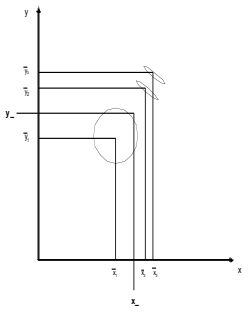

Figure 70 Centroid Calculation

Finally, Figure 70 shows the calculations shown in Figures 68 and 69 combined to calculate the overall area centroid as noted by $(\tilde{X},\tilde{Y})$. This position is the calculated focal spot location. As shown in Figure 70, the image of the central flat plate will have a significant "blob" of light located at the center of the sensor as the control described in this dissertation assumes a coarse focus is obtained before the methods of this paper are used for fine focus. If the "blob" of light in the center of the image is too big for the area centroids to be calculated, it can be suppressed in the calculation of centroids to obtain locations that are very close to focus.

Experiment 4

Figure 71 depicts the setup used for collecting images for analysis. The source of light used was a 3 inch

diameter red LED taillight. The size of the light gives an extended source a little over half of the Sun's diameter as viewed from the concentrator. For the setup shown in Figure 71, the size of light that corresponds to Earth's orbit is approximately 5 inches in diameter. SRS Technology's 1X2 meter elliptical concentrator was used to focus light on the thruster/absorber and secondary concentrator as well as the later imaging of the single loop of tubing utilized in the study of misalignments closer than 2-3 diameters off of focus.

Images were obtained using a STX-10XE CCD camera from Santa Barbara Instrument Group (SBIG). This camera provides a 2184 X 1472 pixel 6.8□CCD for imaging. CCDOPS from SBIG was used on a notebook computer to acquire images at 0.5 sec exposure times. The Sun simulator was connected to a tripod which allowed the Sun simulator to move around at the second focal spot of the concentrator providing the misalignment of the Sun and the concentrator for study. Images were then taken with the Sun simulator at various locations from focus in 1 diameter increments. The maximum distances that were obtainable in the physical layout shown in Figure 71 was 3-4 diameters off of focus in the X direction and 2-3 diameters in the Z direction. Movement in the y direction was not checked in these experiments.

Figure 72 and Figure 73 show the actual equipment used in the experiments. The assigned coordinate axes for the light source are shown in Figure 74 and in Figure 75 for the thruster in these experiments. These coordinate systems become more important for control of the hexapod used for moving the concentrator.

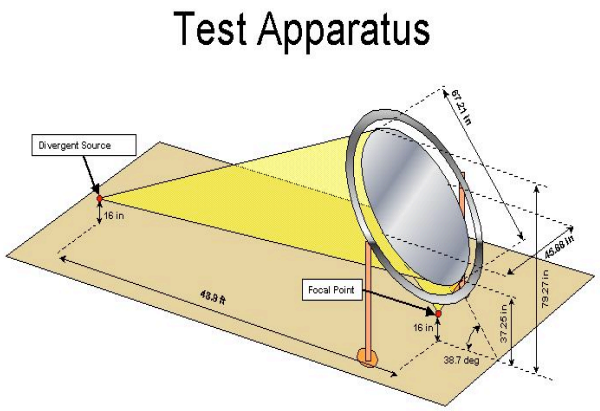

Figure 71 Test Setup

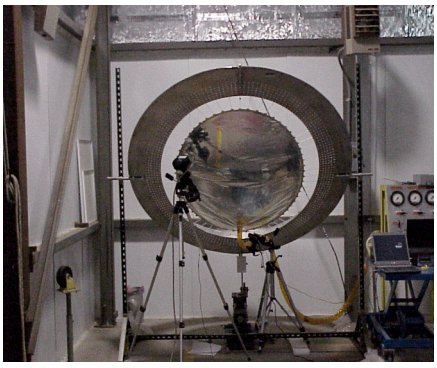

Figure 72 Concentrator From Source End

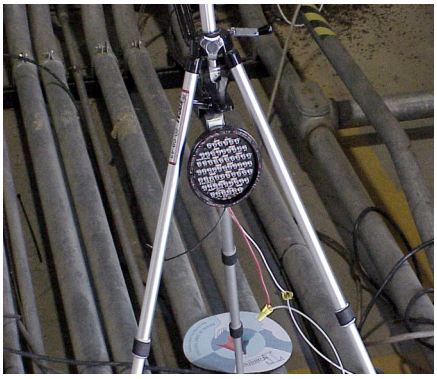

Figure 73 Divergent Source

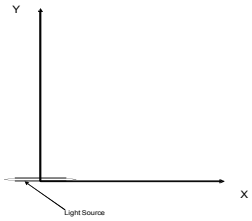

Figure 74 Top View Coordinate System for Light Source

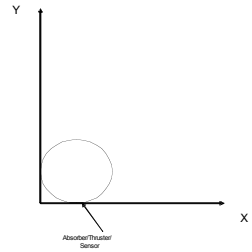

Figure 75 Top View Coordinates at Thruster

ImageJ and Image Analysis[xxii]

The ImageJ image analysis and processing package from the National Institutes of Health was used to process the images taken in the experiments. The program provides a Graphical User Interface (GUI) and extensive image analysis commands. ImageJ is also extendable by using either macros

or ImageJ plugins. Plugins are basically Java classes that implement one of several interfaces in ImageJ or they are Java classes performing specific operations within ImageJ.

Method 1

ImageJ performs correlation on images using the conjugate multiplication of the Fourier transforms of two images to be correlated. Masks were utilized to reduce the size of images to include only the absorber area as the region of interest. Masking also helped the processing time required for the calculation of the FFTs as the images were reduced from 2184 X 1472 down to a more manageable 512 X 512 while still maintaining the correct region of interest. Results from the processing of various offsets from on-focus are presented in Figures 76 through 79. Figure 76 shows the autocorrelation result for the on-focus image. It has a very clear "dot" or impulse at the center of the image. This result was expected as the autocorrelation of an image with itself would be an impulse at offset (0,0).

Figure 77 shows the result for the cross-correlation between the images for up 1 diameter from on-focus of the solar simulator and the on-focus. In this instance, the correlation is smeared and basically located at the center of the image indicating that the 1 diameter misalignment

has not been resolved from the on-focus situation in which the maximum value is located in the center of the image.

Figure 78 shows a much better situation for the correlation technique. This Figure shows the correlation between a 4 diameter image and the on-focus image. This Figure also shows the result for a mask similar to the one shown in Figure 66. The mask used for Figure 78 has other problems at a smaller offset as the numbers of correlations that may occur in the image get larger as the focus spot gets closer to the on-focus location.

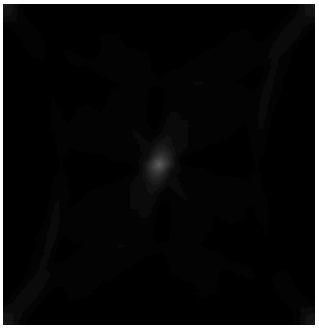

Figure 76 Autocorrelation

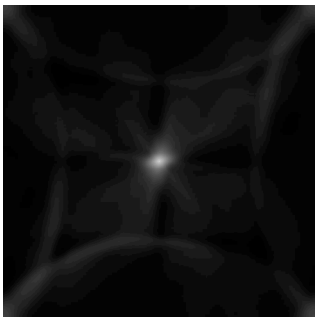

Figure 77 Correlation Up 1 Diameter

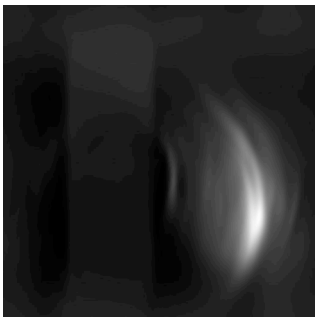

Figure 78 Correlation For a 4 Diameter Offset

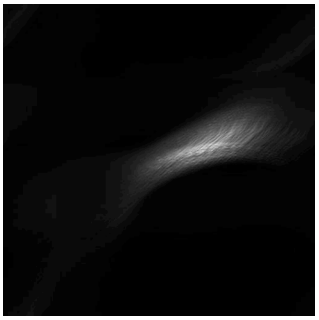

Figure 79 Correlation For a 2 Diameter Offset

The correlation shown in Figure 79 illustrates the problems involved when using the correlation function at offsets below about 3 diameters. The correlation in Figure 79 shows that an offset exists; however, the offset itself cannot be determined from this image. The cutoff for using masks like those in Figures 64 and 65 using correlation defined by Equation 15 appears to be between 2 and 3 diameters of offset.

However, at this point it was noted that using only Equation 15 lead to problems as it would find any and all correlations based on the maximum intensities present, with little regard for the variations in intensities present in

an area of the image, instead of the correct correlation value. That is, Equation 15 would pick an area in I(m,n) that in general had very high intensities instead of actually the point of highest correlation. That problem is eliminated by dividing Equation 15 by the total energy in I(m,n), $\sqrt{\left(\sum_{j=1}^{J}\sum_{i=1}^{I} I^2(i+m-1, j+n-1)\right)}$. Furthermore, Equation 15 can be normalized to the range (-1,1) by dividing by the energy in W(m,n). It was not necessary to divide by the energy of W(m,n) for the case being discussed in this dissertation as it was not important to get values from (-1, 1). Another form for Equation 15 is known as the phase only correlation that basically divides W(m,n) by the magnitude of W(m,n), which normalizes the FFT of W providing only the phase information which provides a more impulse-like function for the correlation. As a quick approximation of the phase only correlation, a high pass filtering was tried since the phase only equation is similar to Equation 15 but with the addition of dividing by the magnitude of W. Dividing by the magnitude of W, with W having low pass frequency patterns, is approximately high pass. However, phase only correlation was abandoned because it did not handle rotations of the region of interest satisfactorily.

Method 2

ImageJ was also utilized for the analysis outlined in method two of this paper. The particular command used was the "Analyze Particles" of the Analyze menu. To prepare the images for analysis, each image had to have a threshold applied before "Analyze Particles" would work. For the experiments in this paper the automatic threshold was used for all images. It was felt that auto threshold would be fine for verifying the concepts and algorithms presented in this paper. Table 4 lists the various particles found in calculating the areas and centroids for each image examined. Particle analysis does not require masking so no masks are indicated. The label column describes the image file which also presents the source positioning information for that image. For example the label "up0diam_1diam_pos_x…" indicates that the source light was positioned 1 diameter off of center in the positive X direction and was not moved vertically, etc. Figures 74 and 75 present the corresponding coordinate axes for both the source and the thruster as used in Table 4.

	Label	Area	X	Y	Major	Minor	Angle
1	on_focus_pt5secs_4_aug_2005	4343	276.746	29.401	182.604	30.282	166.102
2	on_focus_pt5secs_4_aug_2005	16891	292.18	139.54	160.747	133.908	134.72
3	on_focus_pt5secs_4_aug_2005	1175	304.546	429.943	109.479	13.665	14.483

4	up0diam_1diam_pos_x_pt5secs_4_aug_2005	6187	185.416	35.906	183.007	43.066	11.87
5	up0diam_1diam_pos_x_pt5secs_4_aug_2005	27247	258.621	161.973	218.615	158.964	120.044
6	up0diam_1diam_pos_x_pt5secs_4_aug_2005	2705	203.531	424.335	166.181	20.733	164.91
7	up0diam_1diam_neg_x_pt5secs_4_aug_2005	3978	337.551	55.936	173.186	29.253	147.823
8	up0diam_1pt5inch_neg_x_pt5secs_4_aug_2005	5127	314.891	44.521	189.146	34.519	154.33
9	up0diam_1pt5inch_neg_x_pt5secs_4_aug_2005	6695	334.321	130.899	117.068	72.848	133.903
10	up0diam_1pt5inch_pos_x_pt5secs_4_aug_2005	5195	178.505	38.044	168.821	39.188	13.164
11	up0diam_1pt5inch_pos_x_pt5secs_4_aug_2005	28812	253.873	178.983	225.809	162.904	116.247
12	up0diam_1pt5inch_pos_x_pt5secs_4_aug_2005	3686	187.472	418.152	188.46	24.916	161.517
13	up0diam_2diam_neg_x_pt5secs_4_aug_2005	4431	375.153	86.678	182.028	30.994	135.517
14	up0diam_3diam_neg_x_pt5secs_4_aug_2005	4091	383.473	93.188	175.383	29.7	133.809
15	up0diam_2diam_pos_x_pt5secs_4_aug_2005	280	182.303	10.264	30.403	11.894	13.253
16	up0diam_2diam_pos_x_pt5secs_4_aug_2005	3431	69.194	94.311	150.213	29.099	52.783
17	up0diam_2diam_pos_x_pt5secs_4_aug_2005	22244	203.33	195.177	224.069	127.143	121.013
18	up0diam_2diam_pos_x_pt5secs_4_aug_2005	5181	86.968	354.649	210.627	31.325	138.272
19	up0diam_3diam_pos_x_pt5secs_4_aug_2005	1447	45.048	126.181	78.912	23.347	65.158
20	up0diam_3diam_pos_x_pt5secs_4_aug_2005	2634	28.036	295.441	139.366	24.064	119.143
21	up0diam_3diam_pos_x_pt5secs_4_aug_2005	211	176.264	252.713	24.213	11.358	113.949

Table 4 Images and Area Calculations with Centroids and Ellipse parameters.

The columns in Table 4 for major, minor and angle are the parameters for ellipses that approximate the areas of light in the images. These parameters were taken for future analyses that involve using the major axis and minor axis values to determine shrinkage or elongation of the light areas that may be useful to increase the effectiveness of the area moment method for determining focal spot location. The angle parameter is related to the

angle between the major axis of each ellipse and a line parallel to the horizontal or X axis in the image. The angle and the length measurements could be combined into the method of area moments to enhance the focal spot location determination.

Figure 80 On-Focus Image For Area Measurements

Figure 80 presents the situation in the process after the image has been cropped and a threshold has been applied. The next step in the process is shown in Figure 81 when ImageJ has calculated the individual areas based on a minimum size of 100 pixels. The 100 pixel limit came from an approximate value of 2000 pixels that would be in a "tube blob" area calculation for a fully lit concentrator on-focus. The 100 pixel area represented 3-5% of full light, so that we looked for light areas representing 95% fully illuminated concentrator. The values for the

centroids and areas for the image shown in Figure 81 are shown in table 1 with label on_focus_pt5secs_4_aug_2005. Calculations for the image: up0diam_1diam_pos_x_pt5secs_4_aug_2005 gave an average X value of 215.856 and average Y value of 207.405. The method then uses either the centroid of the central "plate blob" of light or the centroid of the on-focus image to generate the difference signal used for concentrator control. For the "tube blob" analysis, the difference calculation gives an X difference of -73.301 and a Y difference of -7.777. By subtracting the focal spot centroids from the centroid of the "blob" a direction of movement towards focus is generated. If the on-focus X and Y centroids are retained from that image a larger displacement value may be generated for the control values that move the focal spot towards focus. When there is no central "plate blob" of light in the image, the centroids for X and Y from the on-focus image have to be used for delta calculations. These delta calculations would then be used to generate control values for the hexapod controller. Looking at Figure 82, it can be seen that this method works down to at least 1.5 inches off of focus for the solar simulator. That number is associated with 0.15 degrees of

offset for the test setup, which is very close to the requirement that we control to 0.1 degree.

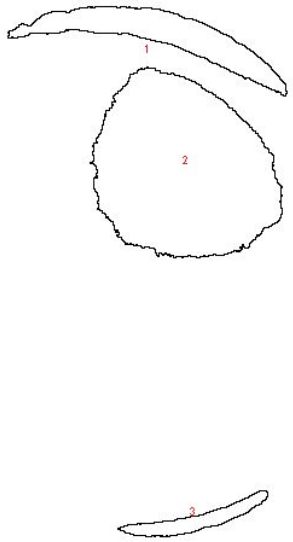

Figure 81 Resulting Particles From 80, Blobs 1 and 3 are Concentrator Images on Tubes

Centroid Results

	Label	Area	X	Y	Major	Minor	Angle
1	on_focus_pt5secs_4_aug_2005	4343	276.746	29.401	182.604	30.282	166.102
2	on_focus_pt5secs_4_aug_2005	16891	292.18	139.54	160.747	133.908	134.72
3	on_focus_pt5secs_4_aug_2005	1175	304.546	429.943	109.479	13.665	14.483
Averages			291.157	199.628			
4	up0diam_1diam_pos_x_pt5secs_4_aug_2005	6187	185.416	35.906	183.007	43.066	11.87
5	up0diam_1diam_pos_x_pt5secs_4_aug_2005	27247	258.621	161.973	218.615	158.964	120.044
6	up0diam_1diam_pos_x_pt5secs_4_aug_2005	2705	203.531	424.335	166.181	20.733	164.91
Averages			215.856	207.405			
Differences (On – 1diam)			73.301	-7.777			

Figure 82 Result of Centroid Calculation

Summary Experiment 4:

Both methods work for locating the focal spot on the sensor. Correlation using only Equation 15 fails to work below 2-3 diameters of misalignment. Test images using high pass filtering to approximate phase only correlation was begun. This method was not fully implemented.

Area moments did better below 2-3 diameters of misalignment. Figure 82 shows the complete calculation for one set of images used in this study. Good focal spot tracking was seen from 5 diameters of misalignment down to 1.5 inch of misalignment. The 1.5 inch gives about 0.15 degree of misalignment, which is very close to our original requirement.

Summary and Conclusions of Dissertation:

A system for locating and controlling the focal spot of a solar concentrator has been developed that capitalizes on in-situ thruster components and non-invasive measurements. Compared to the state of the art sensors described in section 3, the new system provides enhanced capability without the need for a cavity or some other intrusive method of sensing the sunlight. Also, the new system is not limited by temperature considerations as many of the sensors in section 3. The new system consists of a conical shaped absorber doing double duty as the heat

transfer device and as the primary sensor that is imaged by a CCD camera as the measurement device. Both of these considerations show that the sensor developed in this dissertation is superior to state of the art sensors since none of the sensors in section 3 can provide focal spot information for continuous tracking of the Sun. Wave front sensor techniques are introduced and modified to apply to the solar concentrator control problem.

Two methods of tracking the focal spot were then developed by modifying the wave front sensor method. One of the methods developed used a correlation process and masking to locate the focal spot. The correlation process was shown to work down to 2-3 Sun diameters of Sun misalignment. The other method called area moments is developed by modifying the lenslet spots distance measurement to looking at areas of light showing in the image. By calculating an average area centroid, the location of the focal spot can be determined and in turn the direction to move the focal spot can be determined. The area moment method was shown to be useful down to an angle of misalignment of 0.15 degrees. This angle of 0.15 degrees is very close to the arbitrary requirement of 0.1 degrees.

An area for future work is possibly a combination of both methods to overcome the limitations of the correlation method alone. Finally, data should be taken below 1.5 inches of misalignment to verify that the method can get to the .1 degree of misalignment and improve the control down to 0.02 degrees of misalignment where the thruster acceleration could be utilized in the optimization of concentrator location using a combination of correlation and area moments or a refined area moment method.

Appendix A: Section 4.2 Images

Various Photos from the experimental setup

Figure 83 A1 CCD Camera Used ST-6 From SBIG

Figure 84 A2 Camera Location On Strut For Concentrator

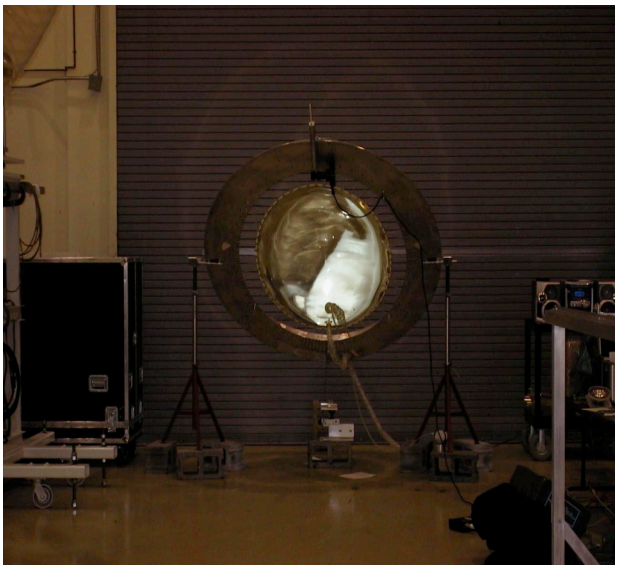

Figure 85 A3 Concentrator In Torus With Camera "on Sun"

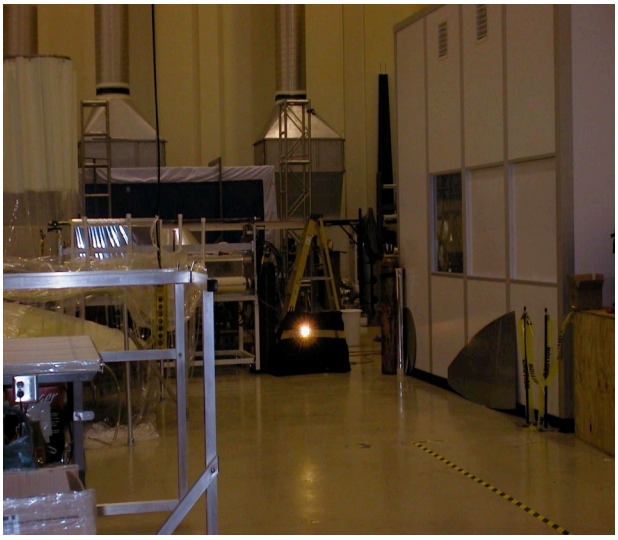

Figure 86 A4 Light Source With Shielding

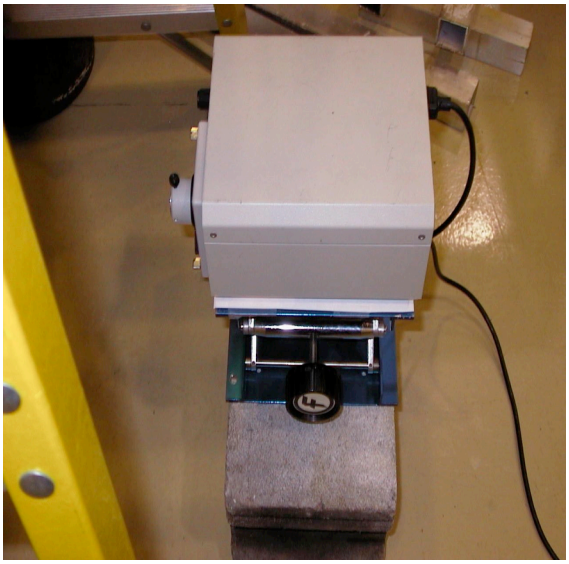

Figure 87 A5 Light Source And Scissor Jack

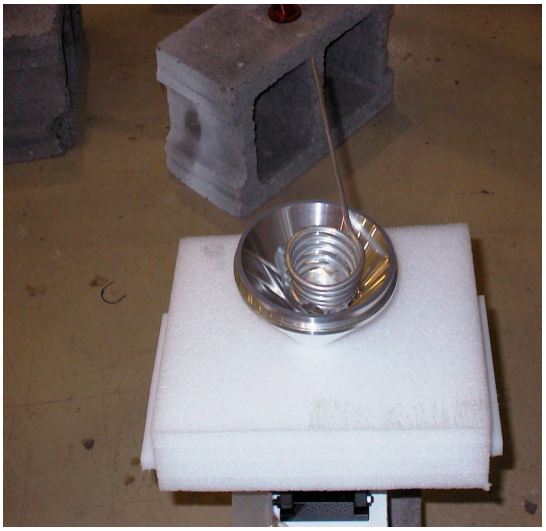

Figure 88 A6 Thruster Holding Table

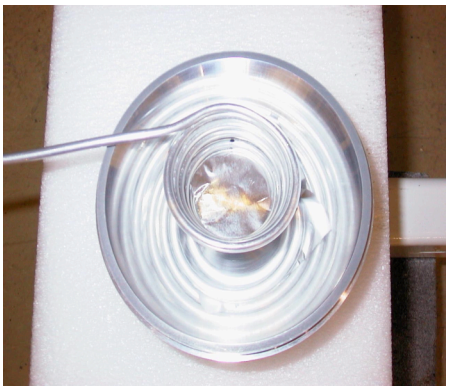

Figure 89 A7 Absorber and Secondary Concentrator

Appendix B: Java Program ConcentratorV3

```
import java.io.*;
import java.math.*;
import javax.media.j3d.*;
import javax.vecmath.*;

public class concentratorv3
{
      public static void main(String[] args) throws IOException
      {
            System.out.println("Hello there!");
            // file io information here
            InputStreamReader reader = new
InputStreamReader(System.in);
            BufferedReader input = new BufferedReader(reader);
            System.out.print("Enter a filename to store results: ");
            String fn = input.readLine();
            System.out.println("This is the file name you gave me: "+
fn);
            //System.out.println("Enter a filename for eij output: ");
            //String fn2 = input.readLine();
            //System.out.println("This is the second file name you gave
me: " + fn2);
            //ends for input of filename.
            int N = 20; //number of points in grid = (2*N-1)*(2*N-1)
            double R = 7.0; //radius of projected circle
            //double f = 7.28;      // focal point location
            double f = 7.28;
            double theta_cone = 30; //half angle of light cone(degrees)
            double phi_cone = 90;   // tilt angle of light
cone.(degrees)
            int li = 0;
            double mzh = 1.52e9;    // sun distance change to correct
val.
            Vector4d[] intensity = new Vector4d[(2*N-1)*(2*N-1)];
            // image of light in concentrator
```

```
            double x =0.0;    double y = 0.0; double thz = 0.48; double
phz = 170.0;
            // x, y are the deltas in phi and theta_c.  thz theta_zhi
and phz phi_zhi
            boolean[] xcirc = new boolean[(2*N-1)*(2*N-1)];// vector to
store logicals defining xs in circle
            Vector3d[] x1 = new Vector3d[(2*N-1)*(2*N-1)];// x1 vector
            Vector3d[] xtemp = new Vector3d[(2*N-1)*(2*N-1)];//  temp
vector
            Vector3d s = new Vector3d(0.0,0.0,f);     //focus vector
            Vector3d st = new Vector3d(0.0,0.0,f);    // copy of focus
vector
            Vector3d sta = new Vector3d(0.0,0.0,0.01);//vector to move
eye
            Vector3d[] eij = new Vector3d[(2*N-1)*(2*N-1)];// pointing
vectors
            Vector3d r,T,zhi; // mirror to Sun vector, reflected
vector, origin to sun vector
            Vector3d[] TT = new Vector3d[(2*N-1)*(2*N-1)];
            Vector3d[] image = new Vector3d[(2*N-1)*(2*N-1)];// image
of sun on focal plane
            Vector3d[] eijtemp = new Vector3d[(2*N-1)*(2*N-
1)];//variable to hold original eij vectors.
            double dth =
(2.0*theta_cone*(Math.PI/180.0))/(2.0*(double)N-1);
            double dphi
=(2.0*theta_cone*(Math.PI/180.0))/(2.0*(double)N-1);
            double zx =
mzh*Math.sin(thz*Math.PI/180.0)*Math.cos(phz*Math.PI/180.0);//vector
components for zhi
            double zy =
mzh*Math.sin(thz*Math.PI/180.0)*Math.sin(phz*Math.PI/180.0);
            double zz = mzh*Math.cos(thz*Math.PI/180.0);
            double costhet = Math.cos(theta_cone*Math.PI/180.0);//used
to make sure eij vectors are all inside the cone of light
            zhi = new Vector3d(zx,zy,zz); //vector from origin to sun
            System.out.println("ZHI = " + zhi);
            Vector3d eoo = new
Vector3d(0,Math.sin(phi_cone*Math.PI/180.0),Math.cos(phi_cone*Math.PI/1
80.0));// e zero zero vector
            System.out.println("E00 = " + eoo);
            Vector3d[] incid = new Vector3d[(2*N-1)*(2*N-1)];//
incident vectors to mirrors
            Vector3d[] norm = new Vector3d[(2*N-1)*(2*N-1)];//normal
vectors
            Vector3d[] nn = new Vector3d[(2*N-1)*(2*N-1)];// copy of
norm values to store
            double cos_sun_t = Math.cos(0.5*Math.PI/180.0);//cosine of
angle of sun disk
            for(int i = 0; i < 2*N-1;i++)
            {
                  for(int j=0;j<2*N-1;j++)
                  {

                        x = ((double)i - (double)N+ 1.0)*dth +
(0.0*Math.PI/180);
                        y = ((double)j - (double)N +1.0)*dphi;
```

```
                        // don't forget to change the x, y below if you
change them here
                        eij[li] = new
Vector3d(Math.tan(x),0,Math.tan(y));
                        eij[li].add(eoo);
                        eij[li].normalize();
                        //System.out.println("eij[" + li + "] = " +
eij[li]);
                        //System.out.println("x = " + x + "y = " + y +
" and zhi = " + zhi + "li = " + li);
                        li++; // increment matrix index
                  }
            }


            // Start of intercept and mirror element calculation
            li = 0;
            st.add(sta);
            st.scale(-1.0);
            double d = 0;
            for(int i = 0;i<2*N-1;i++)
            {
                  for(int j = 0;j<2*N-1;j++)
                  {
                        double a =
(eij[li].x)*(eij[li].x)+(eij[li].y)*(eij[li].y);
                        double b = -4.0*f*eij[li].z;
                        double c  = -4.0*f*f;   // a, b, c from ax^2 +
bx + c = 0
                        d = b*b-4.0*a*c;  //discriminant
                        double t1,t2,t=0;
                        if(a == 0.0) System.out.println("x = " + -c/b);
                        if(d == 0.0) System.out.println("x = " + -
b/(2.0*a));
                        if(d > 0.0)
                        {     //System.out.println("Two real roots");
                              t1 = (-b + Math.sqrt(d))/(2.0*a);
                              t2 = (-b - Math.sqrt(d))/(2.0*a);
                              if(t1 > 0.0 && t2 < 0.0)  t = t1;
                              if(t2 > 0.0 && t1 < 0.0)  t = t2;
                        }
                        if(d < 0.0){
                              System.out.println("Imaginary roots");
                              System.exit(0);
                        }
                        // now find x's which are the mirror element
position vectors
                        x1[li] = new
Vector3d(t*eij[li].x,t*eij[li].y,t*eij[li].z + f);
                        // now find normal vector to each x1
                        nn[li] = new Vector3d(0,0,0);
                        norm[li] = new Vector3d(-
x1[li].x/(2.0*f)/(Math.sqrt(x1[li].z/f + 1.0)),-
x1[li].y/(2.0*f)/(Math.sqrt(x1[li].z/f +
1.0)),1.0/(Math.sqrt(x1[li].z/f +1.0)));
                        //already normalized
                        //
```

```
                        nn[li].add(norm[li]);
                        //System.out.println("norm[" + li + "]= " +
norm[li]);
                        //System.out.println("x1[" + li + "] = " +
x1[li]);
                        incid[li] = new Vector3d(0,0,0);
                        incid[li].add(x1[li]);
                        eijtemp[li] = new Vector3d(0,0,0);
                        eijtemp[li].add(eij[li]);// store original eij
vectors
                        //changed way of calculating incid as original
calc eij vectors only
                        //eij[li].scale(-1.0);
                        //incid[li].add(eij[li]);
                        incid[li].add(st);
                        //System.out.println("incid[" + li + "] = " +
incid[li]);
                        li++; //increment matrix index
                  }
            }
            // now we have arrays of Xs, norms, eyes, and incident rays
            // using the law of reflection, will calculate t, reflected
ray
            // T=incid[li]- 2*(norm[li].dot(incid[li]))*n
            // if T.R / |T|*|R| >= cos theta_sun then "hot"
            // if T.R / |T|*|R| < cos theta_sun then "cold"
            // if "hot" store power of sun portion into intensity
            // generate array of decision values for circular shadow
            li =0;
            for(int i = 0;i<2*N-1;i++)
            {
                  for(int j = 0;j<2*N-1;j++)
                  {
                        if(x1[li].x*x1[li].x+(x1[li].y-
14.81)*(x1[li].y-14.81) <= R*R)
                              xcirc[li] = true;
                        else
                              xcirc[li] = false;
                        li++;
                  }
            }


            li = 0;
            double talpha = 0.0;
            double dottn = 0;
            //open file
            try
            {
            FileWriter out = new FileWriter(fn);
            BufferedWriter brOut = new BufferedWriter(out);
            for(int i = 0; i < 2*N-1;i++)
            {
                  for(int j = 0; j<2*N-1;j++)
                  {
                        x = ((double)i - (double)N+ 1.0)*dth +
(00.0*Math.PI/180);
```

```
                        y = ((double)j - (double)N +1.0)*dphi;
                        //System.out.println("x = " + x + " y = " + y);
                        //System.out.println("li = " + li);
                        r = new Vector3d(0,0,0);
                        T = new Vector3d(0,0,0);
                        intensity[li] = new Vector4d(0,0,0,0);
                        image[li] = new Vector3d(0,0,0);
                        xtemp[li] = new Vector3d(0,0,0);
                        TT[li] = new Vector3d(0,0,0);
                        xtemp[li].add(x1[li]);
                        xtemp[li].scale(-1.0);
                        r.add(zhi);
                        r.add(xtemp[li]); //calculate ray from mirror
to sun
                        r.normalize();
                        //incid[li].scale(-1.0);
                        T.add(incid[li]);
                        //System.out.println("T = " + T + "at li = " +
li);
                        //System.out.println("eij = " + eij[li] + "at
li = " + li);
                        dottn = -2.0*(norm[li].dot(incid[li]));
                        norm[li].scale(dottn);
                        T.add(norm[li]);
                        TT[li].add(T);
                        //System.out.println("T = " + T);
                        //System.out.println("R = " + r);
                        talpha = T.dot(r)/(T.length()*r.length());
                        //System.out.println(" i = " + i + "j = " + j);
                        //System.out.println("talpha = " + talpha);
                        if(xcirc[li])
                        {

      if((eijtemp[li].dot(eoo)/(eijtemp[li].length()*eoo.length()) >=
costhet) && talpha >= cos_sun_t)
                        {
                              intensity[li] = new
Vector4d(x1[li].x,x1[li].y,x1[li].z,1.0);
                              image[li] = new Vector3d(x,y,1.0);
                        }
                        else
                        {     intensity[li] = new
Vector4d(x1[li].x,x1[li].y,x1[li].z,0.0);
                              image[li] = new Vector3d(x,y,0.0);
                        }
                        }
                        else
                        {     intensity[li] = new
Vector4d(x1[li].x,x1[li].y,x1[li].z,0.0);
                              image[li] = new Vector3d(x,y,0.0);
                        }
                        //System.out.println("intensity[" + li + "] = "
+ intensity[li]);
                        //System.out.println("image[" + li + "] = " +
image[li]);
                        //write file
```

```
                        //brOut.write(intensity[li].x + "\t" +
intensity[li].y + "\t" + intensity[li].z + "\t" + intensity[li].w +
"\n");
                        brOut.write(image[li].x + "\t" + image[li].y +
"\t" + image[li].z+ "\t" + li + "\t" + "\n");
                        li++;
                  }
            }
            //close file
            brOut.close();
            out.close();
            }
            catch (IOException e) {

            }
            //File write to save incid, T, and norm values
            /*li = 0;
            try
            {
            FileWriter out = new FileWriter(fn2);
            BufferedWriter brOut = new BufferedWriter(out);
            for(int i = 0; i < 2*N-1;i++)
            {
                  for(int j = 0; j<2*N-1;j++)
                  {
                        brOut.write(incid[li].x + "\t" + incid[li].y +
"\t" + incid[li].z+ "\t" + x1[li].x +"\t" + x1[li].y + "\t" +x1[li].z
+"\t" + nn[li].x+"\t"+ nn[li].y+ "\t" + nn[li].z + "\t" +li + "\t" +
"\n");
                        li++;
                  }
            }
            //close file
            brOut.close();
            out.close();
            }
            catch (IOException e) {

            }*/
      }
}
```

References

[i] Holmes, Dr. Michael R., "Ideal Performance of Off-Axis Paraboloid Concentrators for Solar-Thermal Propulsion," ASME 1996

[ii] IBID

[iii] Wassom, Dr. Steven R., "Focus Control System for Solar Thermal Propulsion," 2000 International ADAMS User Conference.

[iv] IBID.

[v] Dickinson, William C., Paul N. Cheremisinoff, Solar Energy Technology Part A, Engineering Fundamentals, Marcel Dekker, Inc., New York, New York, 1980.

[vi] Hulstrom, Roland L., Solar Resources, The MIT Press, Cambridge, Massachusetts, 1989.

[vii] Beasley, Joseph N., "Digital Signal Processing Techniques for Positioning of Off-axis Solar Concentrators," ASME ISEC 2003

[viii] Beasley, Joseph N., "Thruster Imaging Analysis for Control of a Solar Concentrator," Proceedings of 39th AIAA/ASME/SAE/ASEE, Joint Propulsion Conference, 20-23 July 2003.

[ix] Johnson, Andrew E., Yang Cheng, Larry H. Matthies, "Machine Vision for Autonomous Small Body Navigation", Jet Propulsion Laboratory, California Institute of Technology, IEEE.

[x] Gonzalez, Rafael, C., Richard E. Woods, Digital Image Processing, 2nd Ed., Pearson Education, 2002.

[xi] Beasley, Joseph N., "A Novel Wave Front Method used for Tracking Terrestrial Concentrator Focal Spot Location." Proceedings of 52nd JANNAF Propulsion Meeting, 10-13 May 2004.

[xii] Shack, Roland, Dr., Ben C. Platt, Ph. D., "History and Principles of Shack-Hartmann Wave Front Sensing." Journal of Refractive Surgery, Vol. 17, September/October 2001.

[xiii] IBID.

[xiv] Beasley Joseph N., "Computer Program for Solar Concentrator Focus Control," Proceedings of 53rd JANNAF Meeting, 5-8 December 2005.

[xv] Wassom, Dr. Steven R., "Focus Control System for Solar Thermal Propulsion," 2000 International ADAMS User Conference.

[xvi] Dudzik, Michael c. ed., Electro-Optical Systems Designs, Analysis, and Testing. Volume 4, 2nd ed., Ann Arbor, Michigan: Infrared Information Analysis Center Environmental Research Institute of Michigan., Bellingham, Washington: SPIE Optical Engineering Press., 1996.

[xvii] Wong, Robert Y., Computer Pattern Classification and Scene Matching., The Faculty Press, California State University, Northridge, CA, 1981.

[xviii] Fuentes, Henry Arguello, Gonzalez, Oscar Gualdron, Implementation of a 2D Real-Time Correlator Based on a DSP., http://www.techonline.com/community/tech_group/38730 , Techonline, Texas Instruments, October, 3, 2005.

[xix] Tokovinin Andrei A., "Tutorial on Adaptive Optics at CTIO", http://www.ctio.noao.edu/~atokovin/tutorial/index.html , Cerro Tololo Inter-American Observatory, July 10,2001.

[xx] Hibbeler, R. C, Engineering mechanics, statics. Macmillan Publishing Co., INC, New York, New York, 1978.

[xxi] Dudzik, Michael c. ed., Electro-Optical Systems Designs, Analysis, and Testing. Volume 4, 2nd ed., Ann Arbor, Michigan: Infrared Information Analysis Center Environmental Research Institute of Michigan., Bellingham, Washington: SPIE Optical Engineering Press., 1996.

[xxii] Rasband, W. S., ImageJ, U. S. National Institutes of Health, Bethesda, Maryland, USA, http://rsb.info.nih.gov/ij/, 1997-2005.